The Pennsylvania State University

The Graduate School

Department of Engineering Science and Mechanics

FABRICATION AND TESTING OF PIEZOELECTRIC BISMUTH TITANATE FOR USE AS A HIGH TEMEPRATURE ULTRASONIC TRANSDUCER

A Thesis in

Engineering Science

by

Clifford Searfass

Submitted in Partial Fulfillment
of the Requirements
for the Degree of

Master of Science

December 2008

The thesis of Clifford Searfass was reviewed and approved* by the following:

Bernhard R. Tittmann
Schell Professor of Engineering Science
Thesis Advisor

Dinesh Agrawal
Professor of Engineering Science and Mechanics and
Professor of Materials Science and Engineering

Albert E. Segall
Professor of Engineering Science and Mechanics

Judith A. Todd
Professor of Engineering Science and Mechanics
P.B. Breneman Department Head
Head of the Department of Engineering Science and Mechanics

*Signatures are on file in the Graduate School

ABSTRACT

Bismuth titanate ($Bi_4Ti_3O_{12}$) is a material with potential use as an ultrasonic transducer in high temperature (>400 ^oC) environments and as a replacement of lead containing materials such as lead zirconate titanate compounds. The objective of this study is to validate bismuth titanate for use as an ultrasonic transducer in ambient conditions and at elevated temperatures. This includes testing the capabilities of generating longitudinal, Lamb, and Rayleigh waves.

A spray on sol-gel deposition technique of bismuth titanate is adapted and used for material fabrication because it eliminates needs for ultrasonic couplants at high temperatures and shows promise for use in the evaluation of structures with complicated geometries. Substrate adhesion and transduction efficiency are improved by incorporating microwave sintering and high intensity ultrasonic mixing into the fabrication process. Tested sample substrates include stainless steel and titanium.

Tested samples show large preference to generate vibration modes in the direction of strongest polarization. This makes bismuth titanate an excellent candidate as a longitudinal wave transducer. Longitudinal wave transducers with signal-to-noise ratios as high as 64 dB have been fabricated. Results presented in this thesis show that longitudinal wave transducers can achieve operation up to 680 ^oC and Lamb wave transducers can achieve operation up to 617 ^oC.

TABLE OF CONTENTS

LIST OF FIGURES

LIST OF TABLES

ACKNOWLEDGEMENTS

I would like to thank my father Dave, my mother Linda, my brother Dave, and my grandparents Doris and Elwood Gardner for all their financial and emotional support over all these years. Without them I probably never would have made it this far academically. I would also like to thank Dr. Bernhard R. Tittmann for letting me work in his lab since my undergraduate career and giving me all the great opportunities I've had here at Penn State.

I would also like to thank all my friends. Thanks to Dr. Matt Kropf with his help on various portions of this project, Sean Pursel for taking SEM images and offering his advice with materials fabrication as well as his help with electrode deposition, David A. Parks with his help in high temperature experiments and waveform identification, Kerry Wells and Guneet Sethi for their help with thin film sputtering and my other Engineering Nanostructure Characterization Center lab mates Ryan Pfaff, Dr. Mike Pedrick, Dr. Jikai Du, Katie Boudreau, John Mulry, Brian Reinhardt for his work writing dispersion curve code, Manton Guers and Sahar Louyeh. I would also like to thank my other friends Juan Augustine Melendez, Jon Pitt, Chandan Kumar, Mike Motyka, Brian Murtha, Steve McHale, and Emily Meixell for their support, though mostly non-technical, has been just as important to me. Of course I would also like to thank my girlfriend Erin for reasons she knows why and more.

I would also like to thank Joe Kearns, Dr. Jiping Cheng and Dr. Dinesh Agrawal of the Penn State Microwave Processing Center for training me on their various microwave ovens and allowing me to use them. I would also like to thank Jeff Long,

Maria DiCola and the rest of the staff at the Penn State Materials Research Institute for all their help, and Dr. Mark Horn, Scott Kralik and Ardell Hosterman of the Department of Engineering Science and Mechanics.

I would like to dedicate this to my grandparents Doris and Elwood.

Chapter 1

Introduction

1.1 The Piezoelectric Effect

Materials capable of storing electric energy are classified as dielectrics. Microscopically these materials possess this quality because of the fact that upon the application of an external electric field internal and bound charges displace against molecular and atomic forces [1]. This effect has the mechanical analog to the compression of a mass resting on a spring. As the negative and positive charges shift accordingly to the direction of the electric field a dipole moment is generated; this in turn results in a polarization of the material. Dielectrics containing intrinsic polarization (or spontaneous polarization) are termed polar, while those that do not are aptly referred to as non-polar. Polar materials whose polarizations can be reversed by an applied electric field said to be ferroelectric. All ferroelectrics also belong to a class a materials which are said to be piezoelectric.

Materials that mechanically strain linearly when an electric field is applied are said to exhibit the converse piezoelectric effect (materials which strain quadratically with applied electric field are electrostrictive). Materials exhibiting the converse piezoelectric effect also exhibit the direct piezoelectric effect which is the polarization of a material when it is stressed. In more general words, a piezoelectric material is a material that

generates a net charge when stressed (piezo coming from the greek piezin, or pressure) or conversely strain upon the application of an external electric field.

The piezoelectric effect was first discovered by Pierre and Jacques Curie in 1880 while studying materials such as ferroelectric Rochelle salt and quartz. The Curies later demonstrated the converse piezoelectric effect after Lippmann theoretically predicted its existence from thermodynamic principles [5]. With World Wars I and II and the advent submarine warfare piezoelectricity received much more attention and research because of its potential use in sonar. As a result more materials that transduce more efficiently, like barium titanate, $BaTiO_3$ and lead zirconate titanate (PZT) were discovered. Since then piezoelectrics have found wide ranges of applications such as signal filters, speakers, receivers, transformers and capacitors.

Atomically, the piezoelectric effect is the result of the anisoptropic nature intrinsic to piezoelectric materials crystallographic structure. More precisely, it is a necessary condition for a piezoelectric material to lack symmetry in its atomic crystal structure such that there is a net polarization [6]. The effect is such that an applied strain causes cation/anion displacement resulting in the polarization of the material. Likewise, applied electric fields impose a force on the cations/anoins creating a strain [2,3]. This effect is illustrated in Fig. 1.1. In Fig. 1.1**,** (a) is a two dimensional illustration of a single domain of bismuth titanate, $Bi_4Ti_3O_{12}$, with red, white and black representing the bismuth, oxygen and titanium atoms, respectively. Here the lack of symmetry can be observed from the location of the titanium atom. In (a) the arrow indicates the direction of materials spontaneous polarization. In (b) the lattice is strained creating charge.

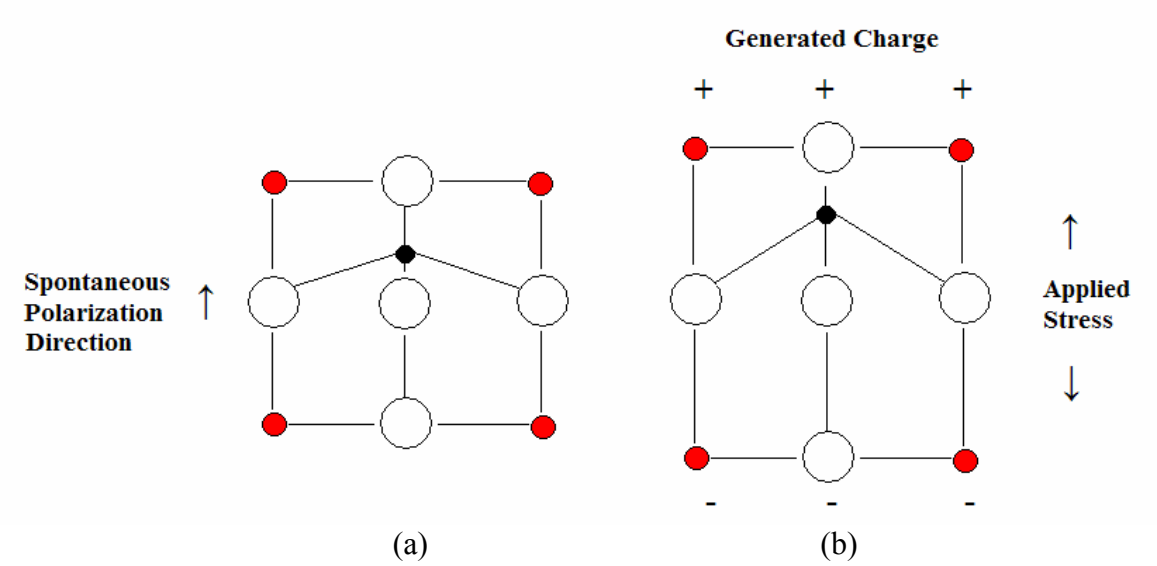

Fig. 1.1 Two dimensional illustration of bismuth titanate ($Bi_4Ti_3O_{12}$) single domain; (a)unstrained and (b) under a tensile load. Figure adapted from [4].

In the generation of ultrasonic waves, piezoelectrics find applications as actuators or receivers. In active applications a voltage pulse or tone burst signal is sent to a piezoelectric transducer. Through the converse piezoelectric effect the electromagnetic signal is converted into a mechanical vibration which travels as an elastic wave. From the direct piezoelectric effect the ultrasonic wave can then be transformed back into an electric signal by another piezoelectric transducer (through-transmission mode) or the same transducer can be used to detect reflected signal (pulse-echo). With proper signal analysis one can determine physical properties such as the acoustic wave velocity of the material (and thus other material properties such as its modulus or density), determine if the material has defects within it, or perform imaging of the samples surface and interior. An illustration of the principle of a transducer operating in pulse-echo-mode is shown in Fig. 1.2. On the left is the physical experimental setup and the right represents an

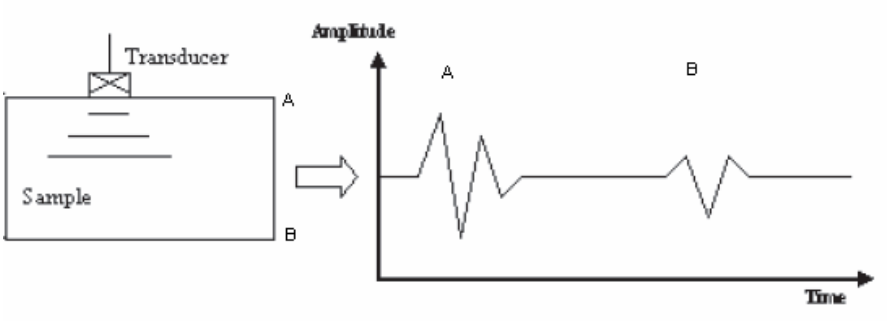

Fig. 1.2: Illustration of the operating principles of transducer. Point A represents the launching of the elastic wave and B is the wave reflected from point B.

idealized received signal. The signal spike at A represents what is known as the "break-through signal", or the time the ultrasonic wave enters the material, and B represents the ultrasonic wave reflected at point B and detected by the transducer again after it has traveled back to point A.

This type of analysis of a material is advantageous because it allows for one to analyze a material without physically having to harm it (e.g. without having to cut it open). Hence this type of structural evaluation is often referred to as non-destructive evaluation. It can also allow for remote analysis of a hazardous system by using guided wave phenomena or wireless technology.

1.2 Temperature Dependence, Electric Domains and Poling

As mentioned previously, a necessary condition for a material to be piezoelectric is for its crystal structure to lack central symmetry. However the atomic orientation/phase of a material is temperature dependent and for piezoelectrics there are temperature ranges for which the material retains this lack of symmetry. The temperature

Table 1.1: Curie-Weiss Temperatures for Several Materials

Material	Curie-Weiss Temperature (^{o}C)
PZT-5H	210
Keramos Lead Metaniobate	400
Bismuth Titanate	685
Aluminum Nitride	1600-1800
Lithium Niobate	1000

where piezoelectricity is lost is known as the Curie-Weiss temperature, or T_c, and above this temperature piezoelectric materials become atomically symmetric and thus lose the piezoelectric effect. Table 1.1 gives some data on Curie-Weiss temperatures for several materials. It should also be noted that depending on the actual efficiency the material has in transforming electrical energy to mechanical energy, and vice versa, the material's piezoelectricity may be too weak to be used practically well before it reaches T_c.

Within a single crystal the anisotropic polarization is uniform throughout the material. In polycrystalline materials, however, this may not always be the case and is usually random. Each grain possesses its own electric domain oriented in a certain direction and the planes at which individual domains conjoin are referred to as domain walls [7]. If the orientation of the domain walls is seemingly random the material will appear to be isotropic and no net piezoelectric effect will be observed. To solve this problem the electric domains within the material must be forced to align. This is accomplished via a process referred to as poling.

In the poling process a material is raised to an elevated temperature, generally around 100-200^{o} C. The elevated temperature provides enough thermal energy that when a large electric field (usually static) is then applied to the material the atoms within each

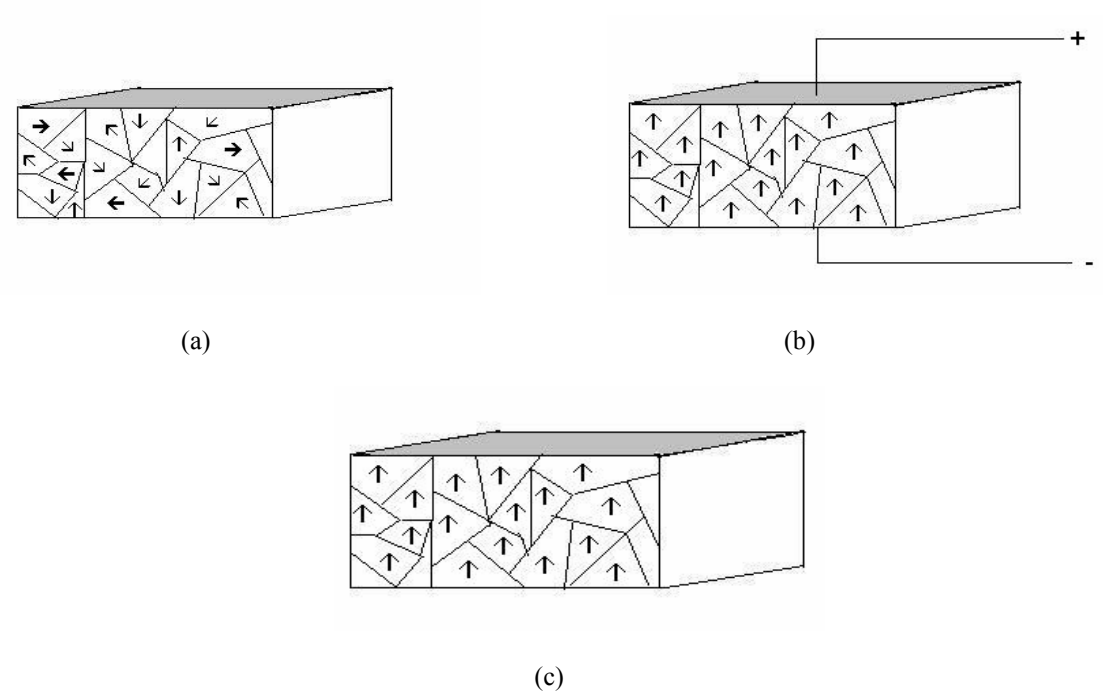

Fig. 1.3: (a) Polycrystalline material before poling, the arrows indicate the random orientation of electric domains within the material. (b) Material at elevated temperature with applied electric field (field is held as sample cools) and (c) cooled material with intact electric domain alignment. Illustrations from Reference [3]

crystal will displace in the proper direction with respect to the electric field. If the field is held as the material cools back to room temperature a net polarization is then induced because not enough (thermal) energy is available for the atoms to reorient themselves to their original positions. Generally the net alignment of grains can achieve 80-90% of the single crystal value [7]. An illustration of the poling process is shown in Fig. 1.3.

One method of poling is done by placing a sample in a heated oil bath. Electrical contacts are brought into contact with electrodes that have been deposited onto the sample and a high voltage is placed over the sample. The oil serves to electrically isolate

the sample (trapping the electric field with the ferroelectric) as well as to heat the material.

Another method of poling is corona discharge poling. This method is advantageous because it does not require the sample to have electrodes however poling uniformity can be a concern because of this. In this technique multiple, thin, sharp (to allow for easy electron emission) conductive needles are brought within a reasonable proximity (e.g. a few centimeters) of the material. The sample and air are then heated, generally to about 200^{o}C. The bottom of the sample is grounded, and a strong electric field is applied to the needles. The elevated temperature allows for atoms in the air to become ionized from the strong electric field and the electrons emitted from the needles resulting in charge conduction. Since the sample is also heated the electric domains are more mobile and can allow themselves to reorient with the direction of the electric field. The electric field remains applied as the sample cools. Fig. 1.4 (a) shows an illustration of the corona poling principle and (b) shows an image of the corona poling setup at Penn State's Materials Research Lab.

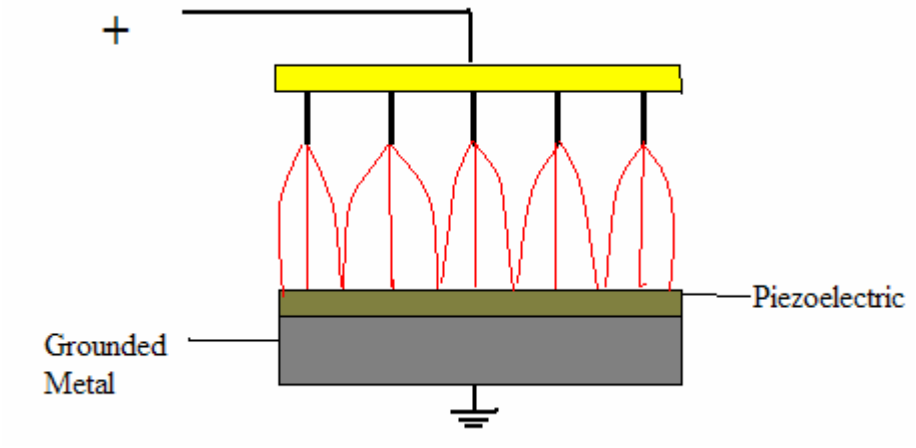

(a)

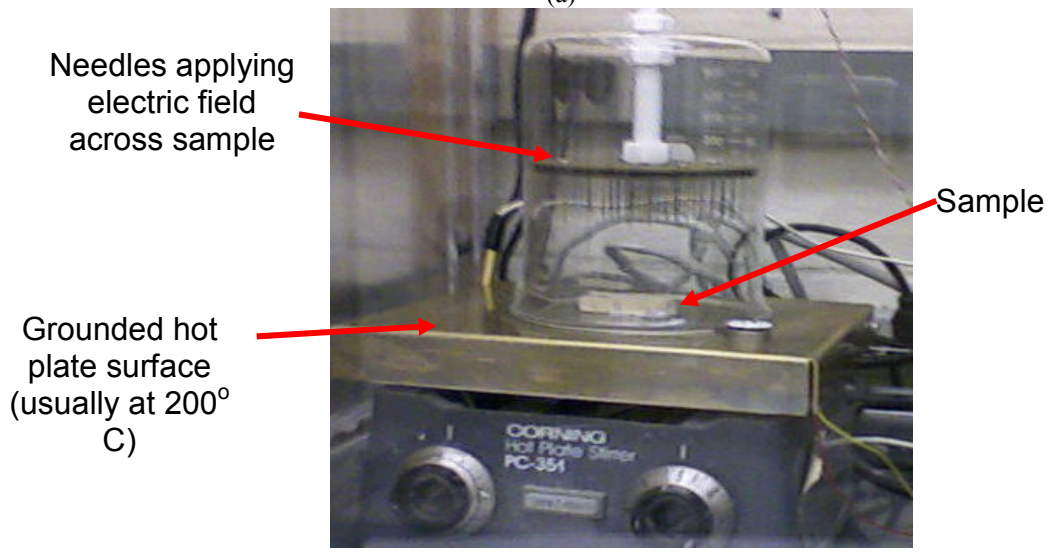

(b)

Fig. 1.4: (a) Illustration of corona poling (red lines represent electric field lines) and (b) image of corona poling setup at Penn State's Materials Research Lab.

1.3 Linear Piezoelectric Equations

The linear equations of piezoelectricity assume that the displacement (u_i) gradient and the electric potential (ϕ) gradient are infitesimal, or

$$\| \frac{\partial u_i}{\partial x_k} \| << 1 \tag{1.1}$$

$$\| \frac{\partial \phi}{\partial x_k} \| << 1 \tag{1.2}$$

Under these assumptions, the strain and electric displacement can then be expressed as

$$S_{ij} = s^E_{ijkl} T_{kl} + d_{kij} E_k \tag{1.3}$$

$$D_i = d_{ikl} T_{kl} + \varepsilon^T_{ik} E_k \tag{1.4}$$

Where s^E_{ijkl} is the fourth order elastic compliance tensor, T_{kl} is the second order stress tensor (applied stress in Eq. 1.3**,** and piezoelectrically induced in Eq. 1.4, ε^T_{ik} is the material permittivity, E_k is the electric field vector (piezoelectrically induced Eq. 1.3**,** and applied in Eq. 1.4), and d_{kij} is a third order tensor that comprises the piezoelectric coefficients. Since d_{kij} is symmetric in i and j, this leaves 18 independent coefficients and invoking proper notation d_{kij} can be expressed as a matrix (i.e. d_{ij} instead of d_{kij}, for further details see [2]). A rigorous derivation of Eq.'s (1.3) – (1.4) from nonlinear electroelasticity theory can be found in [8]. The equations of motion and charge thus become [8]

$$\frac{\partial T_{ji}}{\partial x_j} + \rho f = \rho \frac{\partial^2 u_i}{\partial t^2} \tag{1.5}$$

$$\frac{\partial D_i}{\partial x_i} = \rho_e \tag{1.6}$$

Here ρ_e is the charge density, ρ is the density, and f represents any body forces.

Looking more closely at (1.3) – (1.4**),** it can be seen that the d_{ij} matrix will have units of C/N. Physically this constant represents the conversion of force to charge and vice versa, or, in other words, the ratio of generated strain per applied field or the ratio of short circuit charge per electrode area per applied stress [3]. The j subscript of d_{jk} represents the direction of the electric with respect to the poling axis (3 is always the direction the material was poled in) and k represents the direction of induced strain or applied stress of interest.

One should also note the superscripts on the compliance s^E_{ijkl} and on the permittivity ε^T_{ik}. In the case of the compliance, the superscript E indicates the compliance was measured under the condition that the material was exposed to a constant electric field. If the superscript were a "D" instead, this would mean the compliance was measured at constant charge density, or an open circuit condition. For the permittivity, the "T" superscript indicates the permittivity was measured while the material was allowed to deform. If the superscript was instead an "S", this would indicate that the permittivity was measured while the sample was physically clamped. These constants can be related by the electromechanical coupling coefficient, k, by

$$\varepsilon^S_{jk} = (1 - k^2_{jk})\varepsilon^T_{jk} \tag{1.7}$$

$$s_{jk}^{D} = (1 - k_{jk}^{2}) s_{jk}^{E} \tag{1.8}$$

Thus the stiffness of the material reduces when a sample is electrically shorted, and the permittivity decreases if the sample is clamped. The coupling factor, k^2, represents the ratio of stored mechanical energy to input electrical energy or the ratio of stored electrical energy to input mechanical energy and is therefore by its nature dimensionless [2,9].

1.4 Surface Acoustic Waves (SAWs) and Lamb Waves

In 1885 the existence of surface acoustic waves (SAW waves) were theoretically shown to exist by Lord Rayleigh and therefore they are also commonly referred to as Rayleigh waves [10]. This particular form of vibration is a wave traveling on or close to the surface with its amplitude decaying exponentially with depth. Early in their discovery these wave types were of particular interest to seismologists as these are the principal wave types observed in earth tremors [11]. With the advent of ultrasonic structural health monitoring, SAW waves found application in detection of surface to near surface defects. Modern day SAW devices also find other applications in the electronics industry as filters, oscillators, transformers, and delays.

The following brief derivation of Rayleigh waves is based off of the one presented by Viktorov but for a more in-depth, step by step presentation see the book "Rayleigh and Lamb Waves: Physical Theory and Application."

For a plane harmonic SAW wave traveling on a solid, isotropic elastic half-space occupying the region z>0 and traveling in the x direction; one can show the existence of

Rayleigh waves by first introducing a scalar potential φ and a vector potential $\underline{\psi}$ such that the particle displacement vector $\underline{v}$ can be written as

$$\underline{v} = \underline{\nabla}\varphi + \underline{\nabla} \times \underline{\psi} \tag{1.9}$$

For harmonic processes, the following wave equations are satisfied as

$$\frac{\partial^2 \varphi}{\partial x^2} + \frac{\partial^2 \varphi}{\partial z^2} + k_l^2 \varphi = 0 \tag{1.10}$$

$$\frac{\partial^2 \psi}{\partial x^2} + \frac{\partial^2 \psi}{\partial z^2} + k_t^2 \psi = 0 \tag{1.11}$$

Where $k_l = \omega\sqrt{\rho/\lambda + 2\mu}$ and $k_t = \omega\sqrt{\rho/\mu}$ are longitudinal and transverse wave numbers, respectively, ω is the angular frequency, ρ is the density, and μ and λ are the Lamè constants. Eq.'s (1.10**)** and (1.11) are the decoupled equations governing the longitudinal and transverse components which is characteristic of surface waves. It has been shown that the solutions to this are

$$\begin{aligned} \varphi &= -Ae^{i(kx-\omega t)-qz} \\ \psi &= iA\frac{2kq}{k^2+s^2}e^{i(kx-\omega t)-sz} \end{aligned} \tag{1.12}$$

for $q^2 = k^2 - k_l^2$ and $s^2 = k^2 - k_t^2$, and k coming from the assumed plane harmonic solution. After transforming the characteristic equation for k, the so-called Rayleigh equation is obtained,

$$\eta^6 - 8\eta^4 + 8(3 - 2\xi^2)\eta^2 - 16(1 - \xi^2) = 0 \qquad (1.13)$$

with $\eta = k_t/k = c/c_t; \zeta = k_l/k_t = c_t/c_l$. This equation has 6 roots, with the Rayleigh wave corresponding to the root lying between 0 and 1. This root can be approximated by [12]

$$\eta_R \approx \frac{0.87 + 1.12\nu}{1 + \upsilon} \qquad (1.14)$$

ν being Poisson's ratio. Thus from (1.14), and given the definition of η it is possible to approximate the speed of a surface wave for a given material. Also from Eq. (1.14), since η_R does not depend on frequency, it shows that surface waves are also non-dispersive (at least under the condition that the material is not stressed non-uniformly in any one particular direction and keeping in my mind it is derived from an ideal elastic half space) [11].

Surface waves attenuate rapidly with depth (e.g. on the order of one wavelength) in a material and Eq. (1.12**)** demonstrates this as being exponential. Lamb showed in 1917 that if the thickness of a material (e.g. a plate) approached the order of the wavelength the surface wave degenerates into what are now known as Lamb waves.

For Lamb waves, the potential functions are represented as

$$\begin{aligned} \varphi &= A_s \cosh(qz)e^{i(kx-\omega t)} + B_a \sinh(qz)e^{i(kx-\omega t)} \\ \psi &= D_s \sinh(sz)e^{i(kx-\omega t)} + C_a \cosh(sz)e^{i(kx-\omega t)} \end{aligned} \qquad (1.15)$$

where A_s, B_a, D_s, and C_a are constants, and $q = \sqrt{k^2 - k_l^2}, s = \sqrt{k^2 - k_t^2}$;k, k_l, and k_t being the Lamb, longitudinal and transverse wave numbers. In this situation since the medium is no longer a semi-infinite half space, stress and traction free ($\sigma_{xz} = \sigma_{zz} = 0$)

boundary conditions must be imposed on the top and bottom of the plate. Using these boundary conditions and solving for the constants in Eq. 1.15 two characteristic equations for nontrivial solutions of the wave number k are found as

$$\frac{\tan(\bar{d}\sqrt{1-\zeta^2})}{\tan(\bar{d}\sqrt{\xi^2-\zeta^2})} = -\frac{4\zeta^2\sqrt{1-\zeta^2}\sqrt{\xi^2-\zeta^2}}{(2\zeta^2-1)^2} \tag{1.16}$$

$$\frac{\tan(\bar{d}\sqrt{1-\zeta^2})}{\tan(\bar{d}\sqrt{\xi^2-\zeta^2})} = -\frac{(2\zeta^2-1)^2}{4\zeta^2\sqrt{1-\zeta^2}\sqrt{\xi^2-\zeta^2}} \tag{1.17}$$

where $\bar{d} = k_t d, \zeta^2 = \frac{c_t^2}{c_p^2}, \xi^2 = \frac{c_t^2}{c_l^2}$, d is half the plate thickness and c_p is the phase velocity. Eqs. 1.16 and 1.17 are the solutions for the symmetric and antisymmetric vibration modes (with respect to the middle of the plate). One can solve numerically for the phase velocities from Eqs. 1.16 and 1.17: after which the group velocities can be solved for ($c_g = \frac{d\omega}{dk}$), giving the dispersion curves for a material at a given thickness and frequency. Physically, dispersion of elastic waves is from superposition of the different vibrations upon one another (e.g. shear horizontal waves and shear vertical waves) [15]. A phase velocity dispersion curve for an aluminum plate is shown in Fig. 1.5.

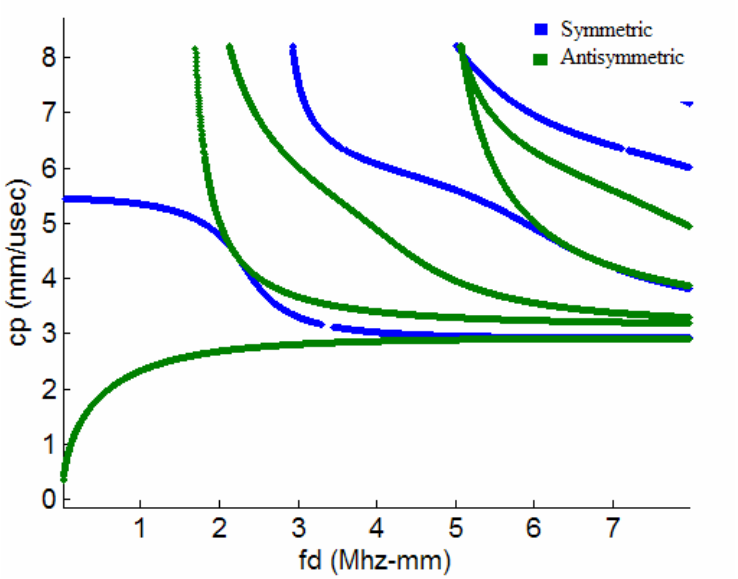

Fig. 1.5: Dispersion curve for an aluminum plate.

Experimentally, surface waves and Lamb waves can be generated by several means. One of the simplest and most effective ways is by using a normal or shear wave transducer placed on a wedge. It is known from Snel's law that $c_1 \sin\theta_2 = c_2 \sin\theta_1$, thus for a Rayleigh wave to be generated $\theta_2 = 90^o$ and the wedge must be at an angle satisfying the condition

$$\sin\theta_w = \frac{c_{1w}}{c_R} \tag{1.18}$$

where c_{1w} and c_R are longitudinal wave velocity in the wedge and surface wave velocity in the material, respectively [15].

Another means of generating Rayleigh or Lamb waves is through the means of a inter-digitized electrode (IDE) configuration. In this technique a periodic array of electrodes are patterned on a piezoelectric material. There are various types of electrode patterns that are used in practice but the most basic is having the electrodes alternate in

applied electrical polarity having spacing equal to twice the wavelength one wants to create. The piezoelectric is placed onto the sample requiring investigation. A voltage signal will generate a deflection with both transverse and longitudinal components in the piezoelectric which carry on into the material. This is illustrated in Fig. 1.6. The red lines illustrate electric field flux lines through the piezoelectric material.

1.5 Bismuth Titanate

Bismuth titanate was discovered by Aurivilius in 1949 [16]. It is a ferroelectric material with the chemical formula $Bi_4Ti_3O_{12}$. It has a high Curie-Weiss temperature, ~685 ^oC, high dielectric constant, ~200, and highly anisotropic conductivity [17-20]. Bismuth titanate has recently been receiving attention because of its potential to replace volatile ferroelectrics such as lead containing PZT, as well as for applications in high temperature environments. Some physical properties of bismuth titanate powders are shown in Table 1.2 [29].

Bismuth titanate has a structure belonging to the so called Aurivilius or bismuth layer structure perovskites, which are crystal structures having a pseudo-perovskite phase that is between $(Bi_2O_2)^{2+}$ layers. The Aurivilius phase family of crystal structures can be represented by the general formula $(Bi_2O_2)^{2+}(A_{n-1}B_nO_{3n+1})^{2-}$; for bismuth titanate n=3 [7,16-18]. This structure for $Bi_4Ti_3O_{12}$ is shown in Fig. 1.7 and a 2-D schematic of its ferroelectric domain is in Fig. 1.1. Above its Curie temperature it belongs to the tetragonal point group having symmetry 4/*mmm*. Below T_c, it can be indexed to either the point group belonging to monoclinic *m* or orthorhombic *mm*2 [17,19,20] .

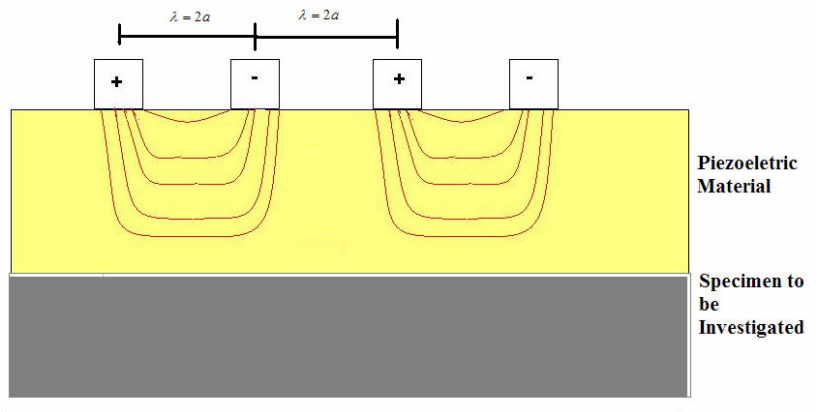

Fig. 1.6: Illustration of surface wave generation using IDE's patterned onto a piezoelectric material.

Table 1.2: Electrical and Mechanical Properties of $Bi_4Ti_3O_{12}$ Powders [29] e

Density ($x10^3$ kg/m^3)	6.55
T_C (^oC)	650
Mechanical Quality Factor Q_M	>600
Maximum Operating Temperature (^oC)	550
Dielectric Constant (1 kHz)	120
Planar Coupling k_p	0.03
Longitudinal Coupling k_{33}	0.09
Piezoelectric Coefficient $d_{31\ (x10^{-12}\ m/V)}$	-2
Piezoelectric Coefficient $d_{33\ (x10^{-12}\ m/V)}$	18

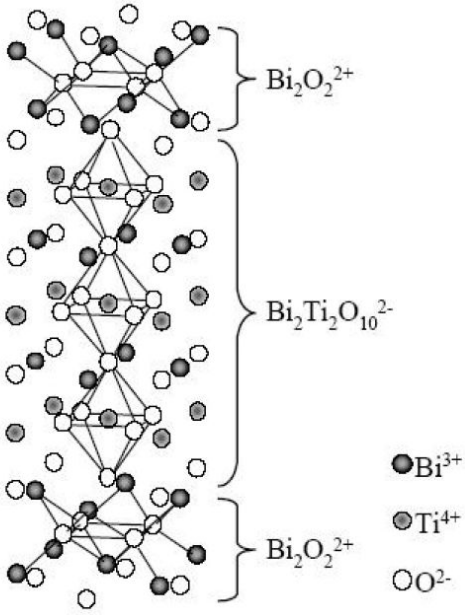

Fig. 1.7: Structure of $Bi_4Ti_3O_{12}$. Illustration from [17]. Reprinted with permission of from IEEE (© 2004 IEEE).

Originally, bismuth titanate ceramics were fabricated using conventional solid state reaction processes. This involves mixing the oxides Bi_2O_3 and TiO_2 and then sintering at elevated temperatures. [17, 21, 22, 23]. Various other thin film techniques such as Physical Vapor Depositoin, Chemical Vapor Deposition, Metal Organic Chemical Vapor Deposition and sol-gel have also been developed [24]. For an extensive overview of the various fabrication techniques see [17].

In the sol-gel procedure one hydrolyzes chemical precursors to form a colloidal solution of the chemical components. For bismuth titanate there are several chemical precursors that can be used and generally these are bismuth nitrate pentahydrate ($Bi(NO_3)_3.5H_2O$) or bismuth acetate ($Bi(CH_3COOH)_3$) and titanium isopropoxide ($Ti(OC_3H_7)_4$. This solution is then dried or milled to achieve the gel. The gel can then be deposited onto the desired substrate and then pyrolyzed to remove unwanted residual

organic compounds leaving an amorphous oxide. Upon sintering, crystallization is induced in the material and takes place through a wide range of temperatures and for bismuth titanate it is almost always above 550^{o}C [17,25 28]. In Chapter 3 this procedure is discussed in more detail.

For high temperature ultrasonic applications the sol-gel technique is advantageous. In high temperature environments, it is hard to acoustically couple transducers to the structure warranting examination. Generally ultrasonic coupling is achieved by the use of gel or oil couplants which are not suitable for high temperature environments. Sometimes acoustic coupling at high temperatures can be achieved through the use of epoxies or liquid metals. Selection of such couplants can be difficult because they require that thermal expansion coefficients be at least on the same order and they also require similar acoustic impedances to allow for wave transmission.

Sol-gel deposition has the potential to eliminate this design problem. If the structure to be interrogated allows for it, that is, it can withstand the sintering process, it can serve directly as the substrate for the piezoelectric material. Therefore the transducer and the structure are then directly mechanically coupled to each other. Another advantage of the sol-gel procedure is that it is potentially easier to analyze complicated structures since the material may be directly deposited onto surfaces of various geometries.

1.6 Microwave Sintering of Ceramics

The microwave region of the electromagnetic spectrum corresponds to electromagnetic waves having frequencies between 0.3 and 300 GHz (1 m < λ < 1mm). Like lasers, microwaves are also coherent and polarized [32]. The polarization and coherence allows for control of the location of the electric and magnetic fields giving one the ability to control the locations of regions with high energy concentration. The direct coupling of microwave energy creates volumetric heating in contrast to surface or interfacial heating found in conventional heating processes. For dielectric materials, the increase in the complex permittivity as a function of temperature accelerates the heating process [31, 32].

The absorption of microwaves by dielectrics and their subsequent heating is attributed to several factors associated with absorption losses. These losses are generally attributed to polarization and conductive processes. In conductive processes, collisions from the motion of ionic and electronic charges generate heat within the material. With polarization processes heat is the by-product of the rotation of electric diploes and short range charge displacement. Polarization losses are also generally attributed to effects associated to interfacial, ionic and electronic polarization. The conductive processes are believed to occur with lower frequency electromagnetic waves at lower temperatures. As frequency increases, the charges travel less distance and have more trouble following the field thus producing less losses and therefore less heat. For losses associated with dipole rotation, lower frequencies are generally absorbed if the material is at a lower temperature and higher frequencies are better absorbed if the material is at higher

temperature [30,31]. These facts are important to recognize since the Federal Communications Commission for industrial, scientific and medical applications has limited microwave heating to a handful of frequencies, namely 0.915 GHz and 28 GHz in North and South America and to 2.45 GHz internationally.

The complex permittivity of a material, ε^*, is often expressed as

$$\varepsilon^* = \varepsilon` - i\varepsilon`` = \varepsilon_0(\varepsilon`_r - i\varepsilon``_{eff}) \tag{1.19}$$

where ε_0 is the permittivity of free space (8.86 x 10^{-12} F/m), $\varepsilon`_r$ is the relative dielectric constant, i is $(-1)^{-1/2}$, and $\varepsilon``_{eff}$ is the effective relative dielectric loss factor. There are many processes associated with microwave losses but it can be difficult to precisely determine which process is responsible for losses at one specific instance. All these losses are generally summed up within the above effective relative dielectric loss, expressed as [31]

$$\varepsilon``_{eff} = \varepsilon``_c + \varepsilon``_s + \varepsilon``_d + \varepsilon``_i + \varepsilon``_e \tag{1.20}$$

The subscripts c, s, d, i, and e corresponding to conductive, interfacial, dipolar, ionic, and electronic losses. The losses from polarization mechanisms are represented in the last four terms of Eqn. 1.20, and for dielectrics absorbing electromagnetic waves in the microwave frequency regime $\varepsilon``_s$ and $\varepsilon``_d$ are the most important. These two factors are also frequency and temperature dependent. The rate of energy absorption per unit volume of a material is dependent on $\varepsilon``_{eff}$ and is expressed as

$$P_a = \omega\varepsilon_0\varepsilon``_{eff}E^2_{rms} + \mu_0\mu``_{eff}H^2_{rms} \tag{1.21}$$

ω and E_{rms}^2 are the angular frequency and rms of the internal electric field, respectively. The second term on the right hand side is associated with magnetic losses and is usually neglected for dielectrics [31]. One can also see from Eq. 1.21 that it is important for the electric field reaching the sample to be of reasonable strength, thus if the sample is held within an insulating holder it is necessary that the holder be microwave transparent. In the case of an oven with a multimode cavity, the sample should be placed in a region of the oven where it is exposed to an electric field with highest and most uniform amplitude.

The losses associated with absorbed microwaves are attributed to conductive and polarization losses which are also frequency dependent. All the samples sintered throughout this thesis were accomplished at 2.45 GHz, and thus the polarization/dipole rotation losses are of the greatest concern. In this process diploes attempt to align with the alternating electric field. As the field dies to zero, the dipoles unalign themselves once again, storing the electric field energy as potential energy which is then released as kinetic and thermal energy [32]. The time it takes a dipole to align and then decay with the electric field is known as the relaxation frequency. The relaxation frequency is a temperature dependent property and therefore so are the polarization losses.

Some dielectric materials absorb little microwave energy at room temperature so heating them with microwaves can be impractical or too time consuming. To overcome this processes known as hybrid heating have been developed to aid with the microwave sintering. One method of hybrid heating involves either the heating of a material via conventional means, such as a furnace, to a temperature where the material has become lossy enough to achieve absorption of the microwave energy. Another means is done by adding material into the sample that is lossier at lower temperatures. A third method is by

using susceptors [30-32]. Susceptors are materials, such as SiC, that absorb microwave energy well at low temperatures. As the susceptors begin to heat the intended sample will be heated by the energy radiated by the susceptors. This will heat the sample until it is lossy enough to absorb to being to heat itself from absorption of the microwave energy.

Illustrations of a typical microwave heating system are shown in Fig. 1.8 . In Fig. 1.8 (a) is the overall setup. A microwave generator generates the microwave, generally using a magnetron or a klystron. The waves are transmitted to the chamber/cavity via waveguides. Reflected power is controlled by a circulator, preventing too much power being reflected to the source protecting it from overheating [31]. Often the chamber may have a vacuum pump system hooked up to it so that microwave processing can be performed in a high vacuum environment or in an environment filled with a certain type of gas such as nitrogen, hydrogen or oxygen. In Fig. 1.8 (b) is a close up of the chamber itself. At the top of the chamber is a quartz window. Through this window one can use a pyrometer or IR thermometer to make temperature measurements of the sample (using these means only a measurement of the surface temperature is possible). The sample holder is placed at the proper position such that the sample will be in good position to absorb the incoming electromagnetic field. The sample holder itself is made of a microwave transparent material such that the microwaves will be not be attenuated when they reach the sample. In Fig. 1.8 (c) is a close up of the sample. Here the susceptors are shown, lying within close proximity of the sample such that it can be heated by the susceptors. The sample holder also serves as an insulator to help keep thermal equilibrium.

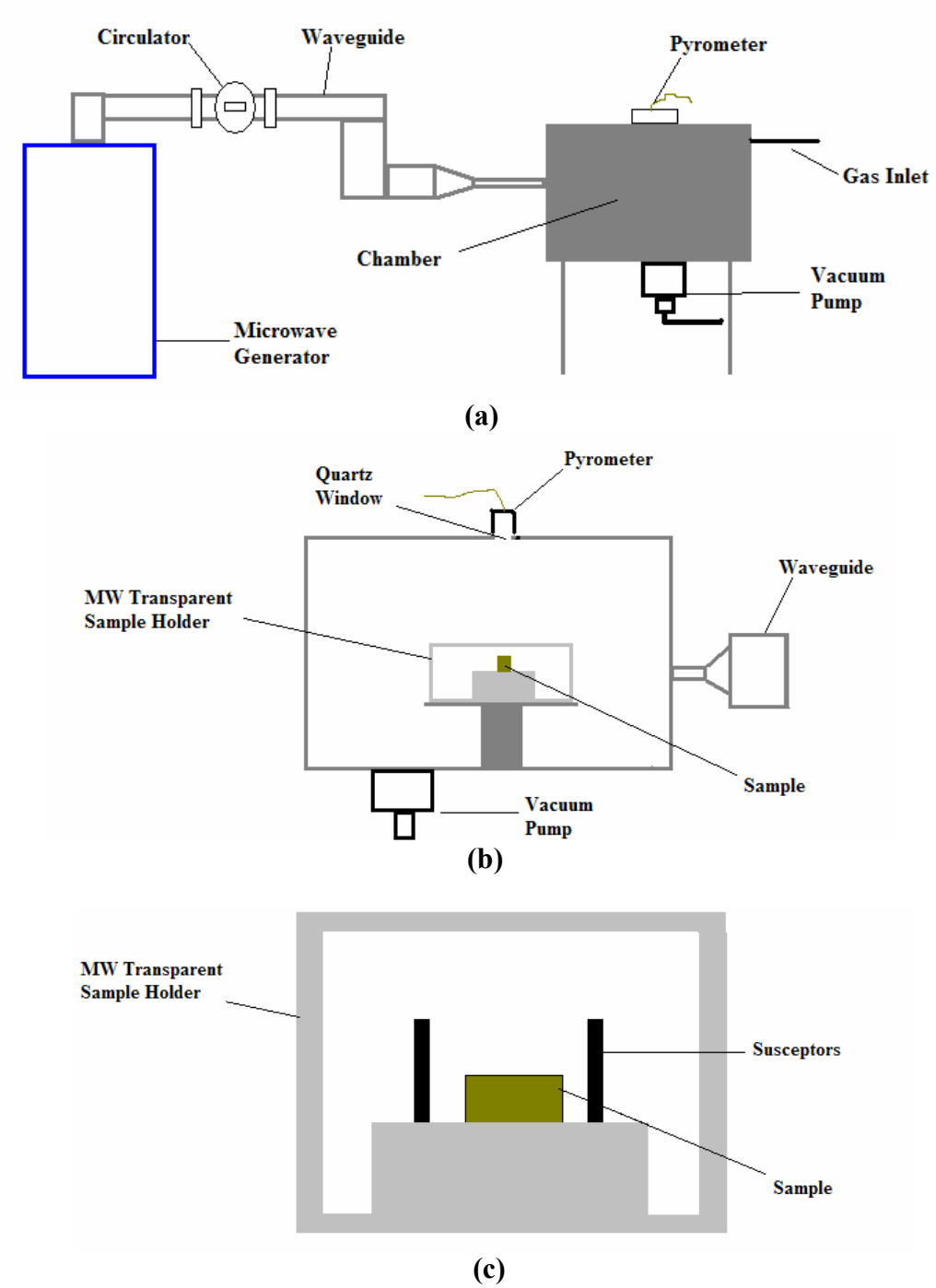

Fig. 1.8: Illustrations of (a) entire microwave setup, (b) close up of the chamber and (c) close up of the sample holder.

Another interesting phenomenon in microwave processing of dielectrics is called thermal runaway. This is the process by which a material experiences unstable accelerated heating. The heating of a material from microwave absorption is the directly affected by $\varepsilon``_{eff}$ and by the materials internal electric field. If the internal electric field within a material is non-uniform or if the material contains impurities (which can also lead to non-uniform internal fields), $d\varepsilon``_{eff}/dT$ will become large in localized regions of the material. As this occurs, the temperature of a material can accelerate exponentially and become unstable. Although a large $d\varepsilon``_{eff}/dT$ is the very reason dielectrics can be heated through microwaves it can also be a problem as far as steady control of sample heating is concerned [31].

1.7 Thesis Objectives and Outline

The main aspect this work is to fabricate and evaluate sol-gel deposited bismuth titanate transducers for applications in the field of ultrasonics. Special focus is given to its capabilities at elevated temperatures. ($T > 250\ ^{o}C$).

The main objectives of this work are to adapt, maximize and implement the sol-gel deposition technique of bismuth titanate transducers. The fabrication techniques involved are presented in Chapter 2. Results of the transducers for practical applications such as longitudinal, Rayleigh, and Lamb wave transducers are examined; these results are shown in Chapter 3. The final aspect of this work is to determine the maximum

temperature capability of bismuth titanate transducers operating in different modes. These results are presented in Chapter 4.

Chapter 2

Sol-gel Fabrication of Bismuth Titanate

2.1 Introduction to Sol-gel Fabrication of Bismuth Titanate

The sol-gel deposition process is a fabrication technique generally applied for making ceramic and glass materials often when thin films of materials are desired [33]. The procedure begins with the mixing of chemical precursors which form the 'sol'. Hydrolysis of the solution forms the gel. More precisely, a sol is a colloidal suspension of solid ions in a solvent, and a gel is a semi-rigid mass formed when the solvent begins to evaporate leaving the particles to begin to form a continuum-like body; pyrolysis and drying produce an amorphous oxide. With further heat treatment crystallization is induced [17,34].

Amongst the first to prepare bismuth titanate via sol-gel deposition was Joshi(1991) *et.al,* Sun (1993,) and Sedlar and Sayer (1995) [25,35,36]. Commonly, acetic acid [CH_3COOH] is used to dissolve bismuth nitrate pentahydrate ($Bi(NO_3)_5.5H_2O$ and titanium isopropoxide [$Ti(OC_3H_7)_4$] is added at constant stirring. Solutions are diluted with H_2O and/or 2-methoxyethanol [$CH_3OCH_2CH_2OH$] can be added to adjust solution viscosity and surface tension. Sun found that highly concentrated solutions were unstable, producing precipitates in short periods of time (about 1 day). The addition of water and/or methoxyethanol increases solution stability [36]. Other authors have demonstrated that bismuth acetate [$Bi(CH_3COO)_3$] reacting with titanium methoxyethoxide

$[Ti_2(OCH_2CH_2OCH_3)_8]$ or bismuth acetate and titanium isopropoxide can also be used as precursors for chemical routes to obtaining $Bi_4Ti_3O_{12}$ [17].

In the separate works by Joshi and Sun, the solutions were spin-coated onto various substrates. The films were then fired between 350-450^o C to allow removal organic matter. Joshi showed that it was possible to achieve crystalline films above annealing temperatures of 550^{o}C [35]. Sun demonstrated that films had the least porosity when sintered between the temperatures of 700-800^o C using conventional methods and raid thermal annealing, with soak times of 2 hours and 30 seconds, respectively [36].

Kobayashi *et.al* were the first to use the basic sol-gel technique described above for depositing thick piezoelectric films for ultrasonic testing purposes [37] . In this method bismuth nitrate pentahydrate and titanium isoproxide were chosen as precursors with acetic acid as the solvent. This solution was then hydrolyzed with the ratio of bismuth titanate solution to water being 2:1. $Bi_4Ti_3O_{12}$ powders were added to the solution and ball milled to achieve gelation. An air gun was then used to spray coat metallic substrates with the sol-gel. Drying, firing and annealing were performed at 90 ^{o}C, 430 ^{o}C, and 700^{o}C respectively, with unspecified time durations and environments. The films had thicknesses of about 80 μm to achieve iltrasonic center frequencies within the rage of 5-30 MHz. The samples were poled using the corona poling discharge method and electroded using a silver paste. The materials were tested up to 200^{o}C where they were found to have a signal to noise ratio of 25 dB.

2.2 Experimental Procedure

In this thesis, the basic procedure for the sol-gel deposition performed mimics that of Kobayashi *et.al* because their method has been shown to be able to produce materials capable of ultrasonic wave generation. Note that the fabrication procedure about to be described in the following paragraphs is also summarized Fig. 2.1.

For the fabrication procedure bismuth nitrate pentahydrate and titanium isopropoxide are the chosen chemical precursors and glacial acetic acid as the solvent. Bismuth nitrate pentahydrate is dissolved in glacial acetic acid at 80^{o} C at constant stirring and then allowed to cool. The proper stoichiometric amount (discussed later in this section) of titanium isopropoxide is then added to the solution. This solution is hydrolyzed with water in a volumetric ratio of solution to H_2O as 2:1. This solution is then allowed to sit for one hour. $Bi_4Ti_3O_{12}$ powders are then added to this solution. The next step in the process (e.g. the powder/solution being ball milled or mixed with an high intensity ultrasonic horn) varies throughout the thesis. Next, using an air gun the mixture is then spray coated onto metallic substrates. In this work the substrates are often stainless steel or titanium. These substrates are then set on a hot plate at 400^{o}C and allowed to sit for 10 minutes or so to evaporate out residual organic compounds. Spraying and heating is then repeated until the desired thickness is achieved.

Once the desired thickness is obtained the samples are then sintered, usually between the range of 700-900 ^{o}C. Samples have been sintered using both conventional and microwave techniques, but, as it is reported in later chapters, microwave sintering has proven itself to be a more superior method.

After sintering samples are then corona poled with the electric field first being applied when the samples reach a temperature of 200^{o} C. Samples are allowed to cool while the electric field remains applied. After corona poling electrodes are applied to the sample surface for testing and oil bath poling. At this point it is convenient to point out that because of the high conductivity bismuth titanate is notorious for being to difficult to pole (i.e. electric breakdown occurs in the sample), and it appears that the corona poling method seems to be successful in helping to overcome this obstacle.

One of the most important steps in the preparation procedure is mixing the chemical precursors, bismuth nitrate pentahydrate and titanium isopropoxide, in the proper molar ratio. The necessary molar ratio has been discovered to be as follows.

In preparation of the solution, bismuth nitrate pentahydrate is dissolved in glacial acetic acid at 80^{o}C. It is known that bismuth nitrate pentahydrate is soluble in weak acids. Given this, its disassociation in the glacial acetic acid should undergo as

$$Bi(NO_3)_3.5H_2O + CH_3COOH \rightarrow Bi(NO_3)_3 + 5\ H_2O + CH_3COOH \qquad (2.1)$$

It is also known that thermal dissocation of $Bi(NO_3)_3$ yields bismuth trioxide and dinitrogen pentoxide [38]

$$2Bi(NO_3)_3 + \text{Heat} \rightarrow Bi_2O_3 + 3N_2O_5 \qquad (2.2)$$

It is well known that titanium isopropoxide reacts with water to produce titanium dioxide (TiO_2) in the reaction

$$3Ti(OC_3H_7)_4 + 6\ H_2O \rightarrow 3TiO_2 + 12\ (CH_3)_2CHOH \qquad (2.3)$$

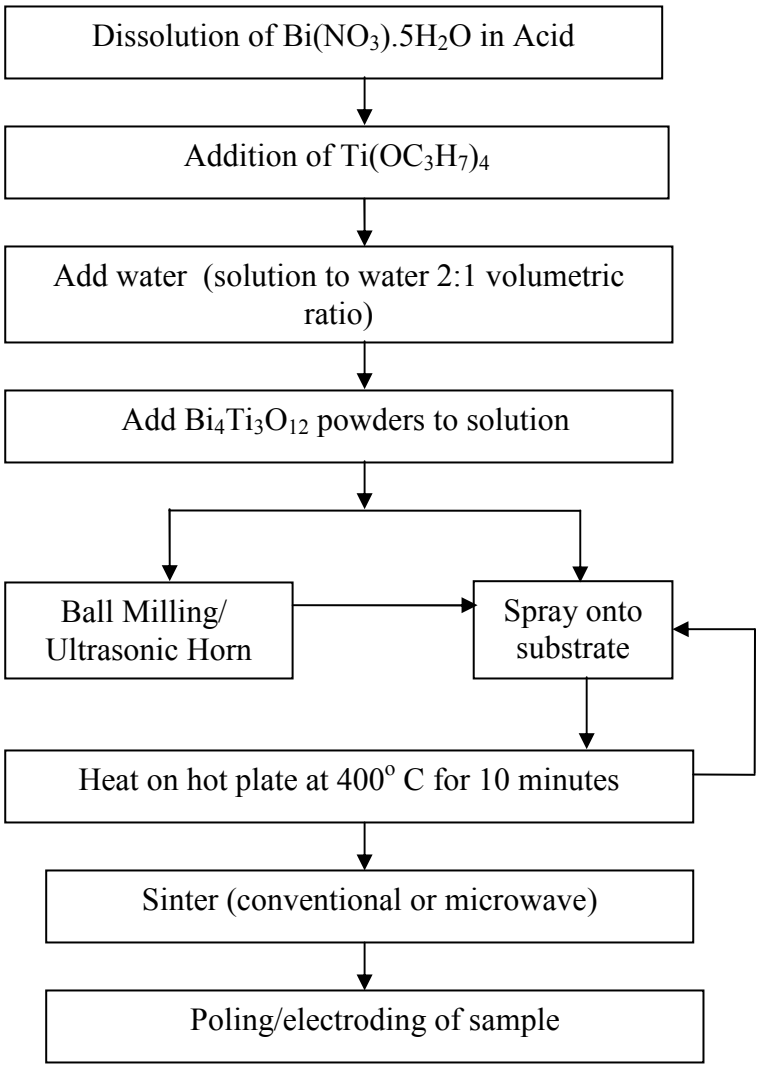

Fig. 2.1: General procedure for sol-gel deposition of $Bi_4Ti_3O_{12}$ samples.

Therefore, combining Eq.'s 2.1, 2.2, and 2.3 and balancing such that Bi_2O_3 and TiO_2 are in the ratio of 2:3, respectively, one obtains 2.4

$$4Bi(NO_3)_3.5H_2O + CH_3COOH + 3Ti(OC_3H_7)_4 \rightarrow 2Bi_2O_3 + 3TiO_2 +$$

$$12\ N_2O_5 + 14H_2O + 12(CH_3)_2CHOH + CH_3COOH \qquad (2.4)$$

It also known that the Bi_2O_3-TiO_2 (in the ratio of 2:3, accordingly, which is what is shown to be produced in Eq. 2.4) system can produce $Bi_4Ti_3O_{12}$ with heat treatment (above ~550 ^oC) giving [39]

$$2Bi_2O_3 + 3TiO_2 \rightarrow Bi_4Ti_3O_{12} \qquad (2.5)$$

Thus, it seems, the solution of chemical precursors provide one with a Bi_2O_3-TiO_2 system that acts as a matrix for the $Bi_4Ti_3O_{12}$ powders, which upon sintering form $Bi_4Ti_3O_{12}$, presumably with the powders acting as primary grains during sintering. Hence the proper molar ratio of bismuth nitrate pentahydrate to titanium isopropoxide is 4:3

Chapter 3

Fabrication of Longitudinal, Rayleigh, and Lamb Wave Transducers

3.1 Fabrication of Longitudinal Wave Transducers

The first samples were fabricated using the basic procedure outlined in Chapter 2.2. The powders used were at a maximum 40 μm in diameter. The first samples to successfully create ultrasonic waves had no special treatment done to the powder/solution mixture (e.g. no ball milling of the mixture). Initially, ball milling had been attempted with tungsten carbide pellets however this procedure seemed to contaminate the solution. This was noticeable by the fact the solution had changed color from an off-white/khaki color to a black/grey color. It is possible this may have occurred from the acid eating away at the tungsten carbide, pieces of the tungsten carbide pellets mixing with the fluid from the strains of milling, or from other contaminants the pellets may have absorbed during their use in previous experiments, despite their extensive cleaning in ultrasonic baths. Images of the first samples to be made prior to sintering are shown in Fig. 3.1.

In the first few attempts, the chosen metallic substrate was steel (except one which is titanium). The samples were sintered in conventional tube furnaces at temperatures in the range of 750 - 850 ^{o}C, with ramp rates of 3^{o}C/min and cool down rates of 3^{o}C/min with soaking times within the range of 1-2 hours. These first samples to be sintered were generally of poor quality. Often, the layer of deposited bismuth titanate had flaked off of the steel before being removed from the oven or had adhesion so poor

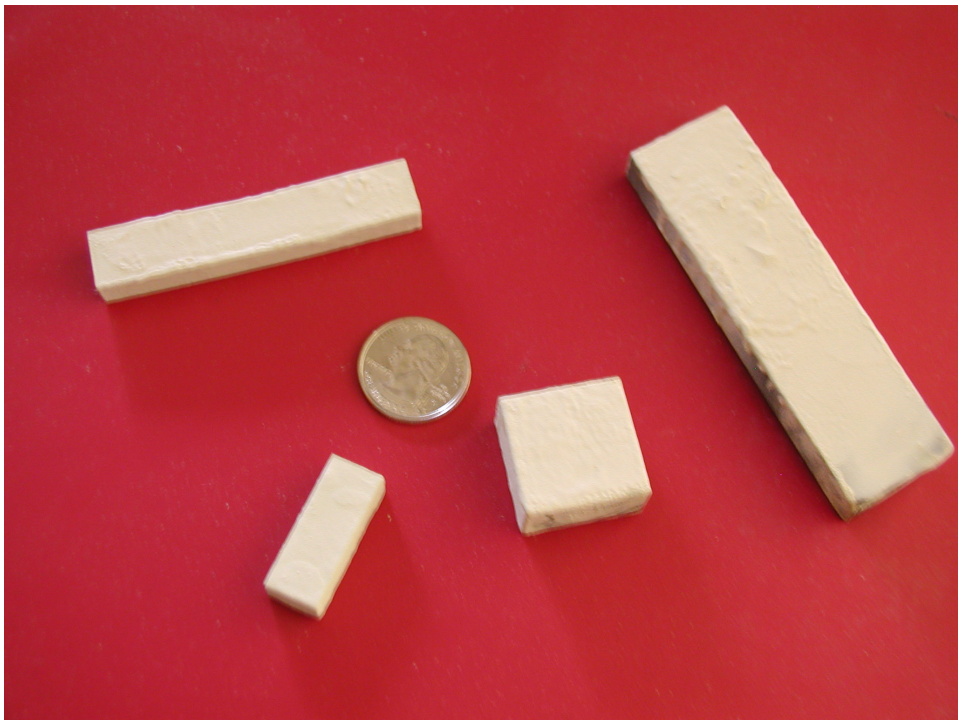

Fig. 3.1: First samples of sol-gel deposited bismuth titanate.

that testing them would destroy the sample and thus were of no real practical use.

It was first believed the poor quality of the first several samples was due to the atmosphere the sintering was performed in since it had previously been reported that sintering of thin film bismuth titanate in oxygen environments produces samples of good quality [26, 28]. Another possible reason for this failure is that the Bi_2O_3 may not have been reacting with TiO_2. The samples were of reddish color, and Bi_2O_3 is known to develop this color after being exposed to high temperatures [38].

The next sample to be sintered had been deposited on a steel substrate 13.4 mm thick. This time the sintering cycle was performed with the sample exposed to a flowing oxygen environment. The ramp rate of this sintering cycle was again 3^o C/min, a soak time and temperature of 20 min at 700^oC and a cool down rate of 3^o C/min. Adhesion of

this sample was enough to allow for poling and testing of the sample. The sample was corona poled in its thickness direction at a temperature of 200^{o} C at a voltage of about 22.5 kV, with the needles being about 7-10 cm away from the sample surface. The measured d_{33} (at 40 Hz) of the sample was between 2-4 pC/N (the value was non-uniform over the sample surface).

For testing the sample for its ultrasonic capabilities conductive tape was used instead of permanent electrodes. This first sample was not capable of producing pulse-echo generation/reception of ultrasonic waves however through-transmission could be achieved with the help of a commercial PZT transducer with a center frequency of 2 MHz. The sample was pulsed at 400 V and the received signal was amplified 60 dB. The waveform is shown in Fig. 3.2. The longitudinal wave velocity of steel is about 6 mm/μs, thus the first wave should be received at 2.24 μs and each successive echo 4.48 μs later.

To try and improve sample quality, the next samples deposited were sintered using microwave furnaces because of their known ability to provide volumetric heating. The first sample was sintered in a 2.45 GHz multimode chamber in an atmospheric environment. Temperature of the sample was measured using a pyrometer and SiC rods with a carbon coating were used as susceptors. A forward power of 1.2 kW was enough to heat the sample to about 850 ^{o}C. These samples also were of poor quality and

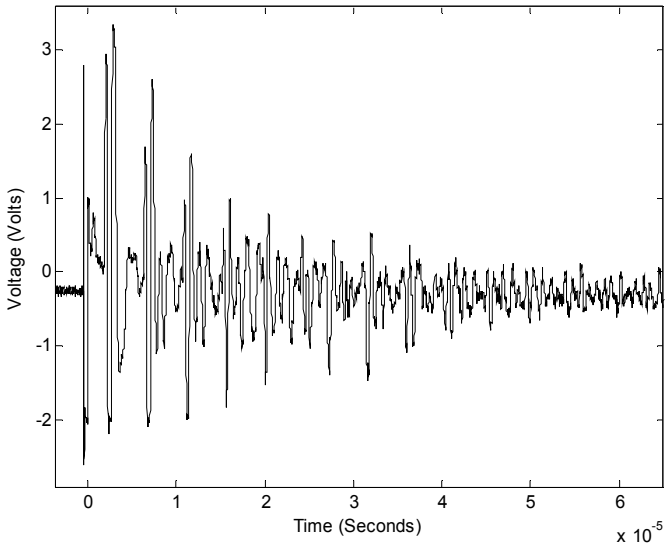

Fig. 3.2: First detected ultrasonic waveform in through-transmission.

were not much better than those sintered in conventional furnaces, and still had a reddish-brown color.

Two ideas were proposed as to why sample quality was so poor. The first was that perhaps contamination was being introduced to the sol-gel during the deposition process. The second was that perhaps the sintering environment was still the problem. Close inspection of the inside of the air gun indicated some possible corrosion of the metal so a new air gun was purchased because it was thought that perhaps the corroded metal could be becoming mixed or be reacting with the solution during the spraying process. The inside of the first air gun was made of either iron or steel. The interior of the second is made of an unknown metal but it suspected that it is brass or bronze; this new air gun has been used many times with no signs of corrosion. Also, a new holder for samples during the sintering process was made. New samples were deposited using the new air gun in the

same fashion as before and sintering was performed in a microwave chamber in a high vacuum environment (>10^{-6} Torr).

The first sample to be sintered had a 7.61 mm thick substrate of titanium. The sintering temperature was once again measured using a pyrometer. The temperature of the sample during sintering was 850 ^{o}C with a soak time of about 10 minutes In this sample adherence of the bismuth titanate to the titanium was superb and almost impossible to remove. The sample was corona poled at 200^{o} C and then tested for its ultrasonic capabilities. Again the sample was corona poled (a d_{33} value of 8 pC/N was measured) and temporarily electroded with conductive tape and was pulsed at 400 V and a pulse echo signal was finally obtained. This waveform is shown in Fig. 3.3. For a 7.61 mm thick titanium (c = 6 mm/μs) the round trip time of flight was estimated to be 2.49 μs.

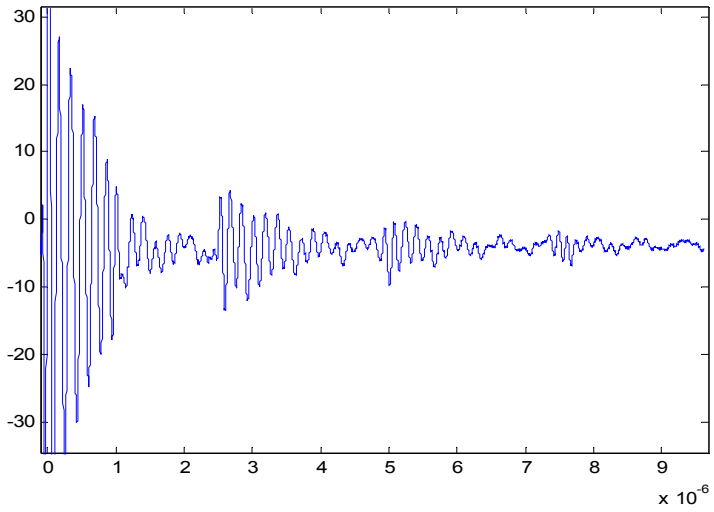

Figure 3.3: Pulse-echo waveform of titanium substrate sample sintered in high vacuum microwave furnace.

To determine whether or not sample contamination or sintering environment had been responsible for the previously poor samples, another sample was prepared and sintered under atmospheric conditions. The sample substrate was a 7 mm thick piece of steel. This sample was sintered at 850^{o} C with a soak time of 10 minutes. This sample also had great structural adhesion between the steel and bismuth titanate. The sample was corona poled (measured d_{33} of about 12 pC/N) and again tested with electrode tape for its ultrasonic capabilities. The generated pulse-echo waveform is shown in Fig. 3.4. Thus it seemed that indeed contamination had been the issue with the previous samples and not the sintering environment (later it was found that the material was magnetic, since

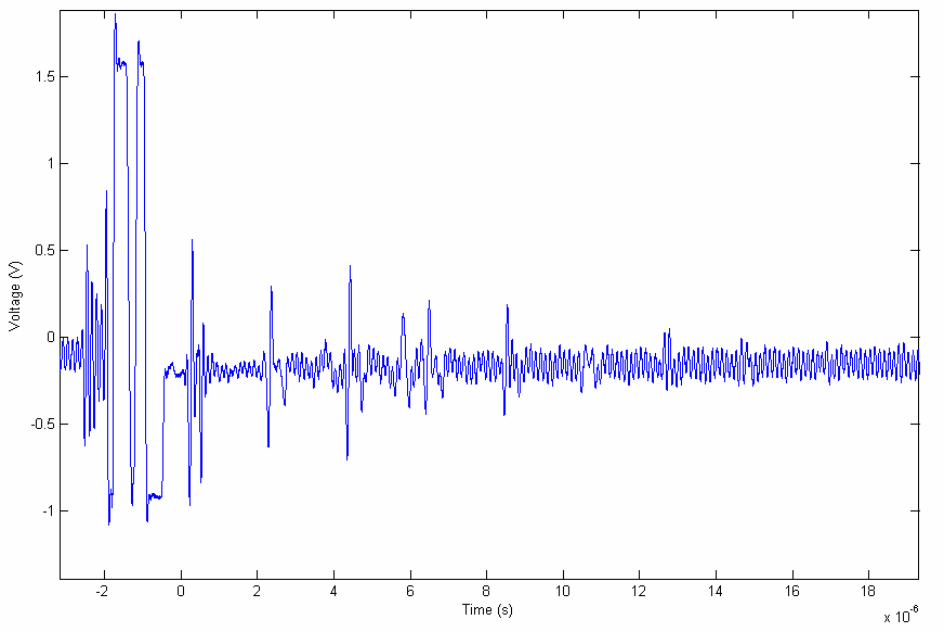

(a)

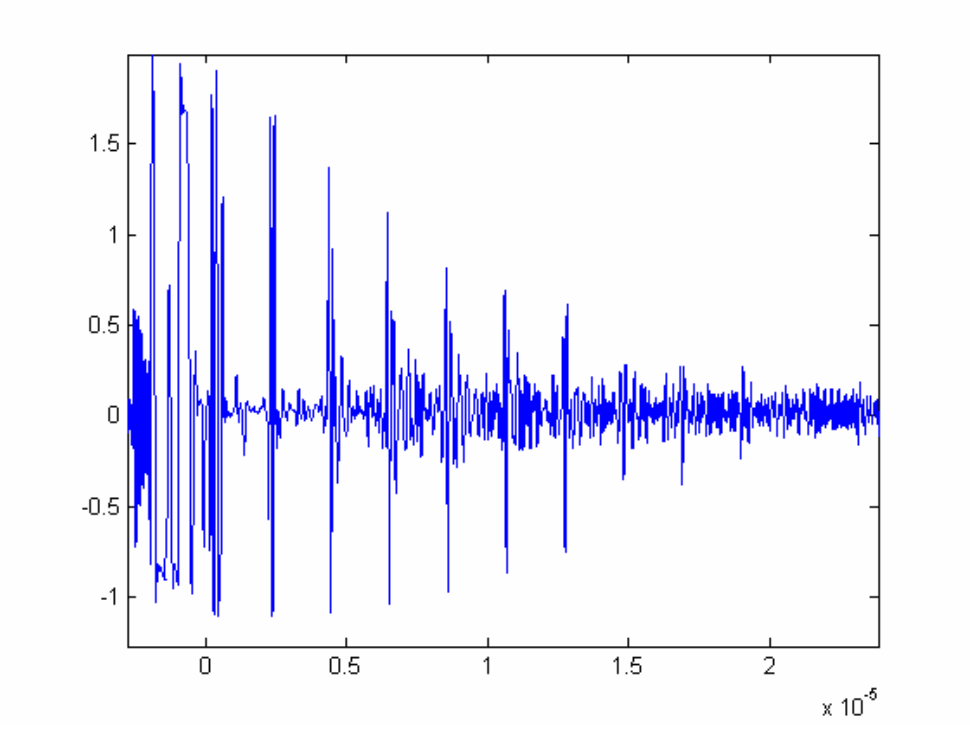

(b)

Fig. 3.4: Pulse-echo waveforms of sample microwave sintered in atmospheric conditions with (a) electrode tape and (b) permanent electrodes.

bismuth titanate is not known to be magnetic it reasonable to assume that the steel from the airgun was somehow reacting with the solution during the deposition process). More samples were later sintered once again in tube furnaces in the same conditions as before and the samples still had poor adhesion to the substrate, indicating that while contamination may have been an issue in later samples (the first samples are presumed to have no contamination since oxidation would have occurred over time) microwave sintering of samples is a better method.

Despite achieving a transducer capable of generating pulse-echo waveforms it was still noticeable that sample microstructure could be improved. This was indicated by the fact that all previous samples had a 'sandy' surface. This was noticed by the fact if one were to run their finger over the sample surface powder from the sample would rub off as well as the fact that porosity was present when viewed under a microscope and sometimes even visible to the naked eye. This was attributed to the fact that some of the powder particles introduced in the mixing stage of preparation were still as large as 40 μm in diameter. Agglomeration of the powders particles was also noticeable when they were introduced to the chemical precursors.

To overcome this, when the powders were introduced to the liquid phase powder/liquid mixture was mixed using a high intensity ultrasonic horn. This visibly reduced particle agglomeration within the liquid and seemed to reduce the average particle size. Figure 3.5 shows an XRD analysis taken of a sample made under these conditions.

Fig. 3.6 shows pulse-echo waveforms from one sample in which this sample preparation technique was employed. In this sample the substrate was a 1.6 cm thick

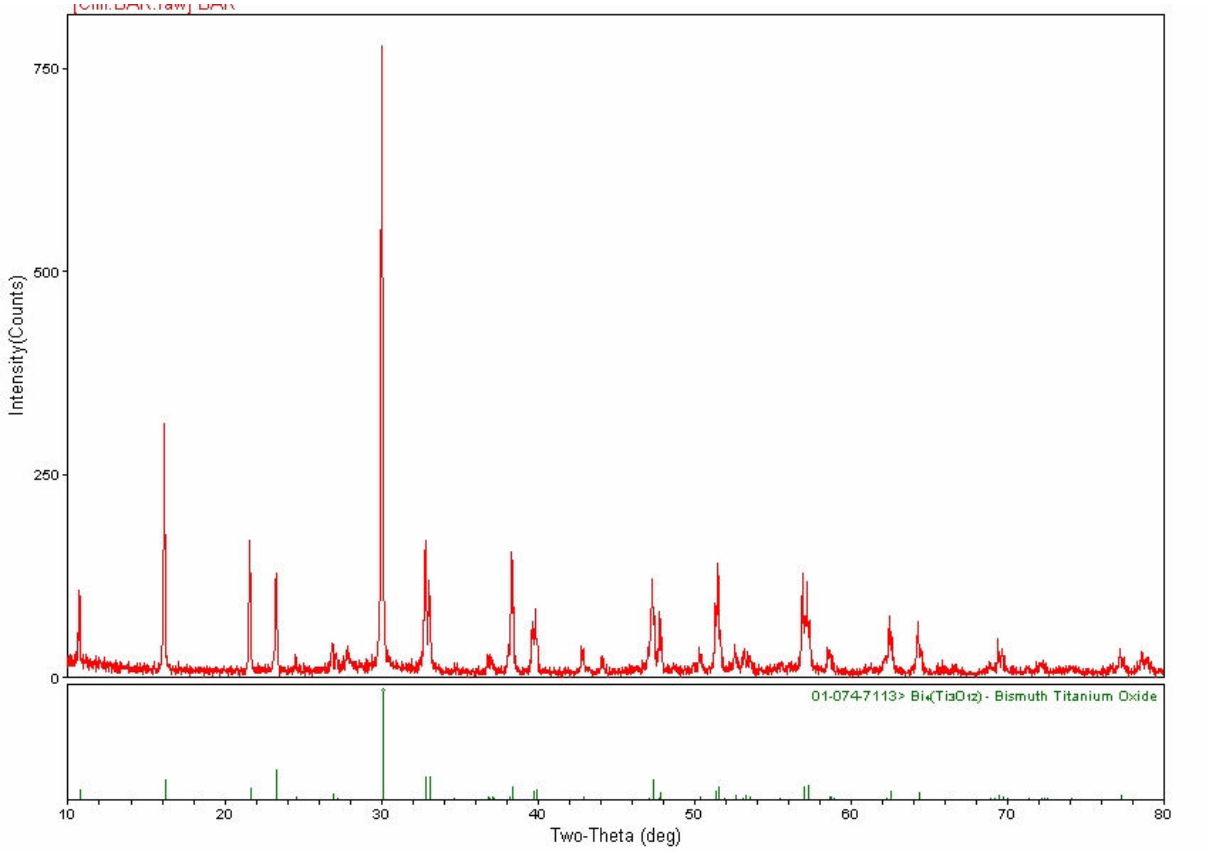

Figure 3.5: XRD analysis of a bismuth titanate sample deposited onto a steel substrate. Top of the figure is the measured spectra and the bottom of the figure is the spectra for $Bi_4Ti_3O_{12}$.

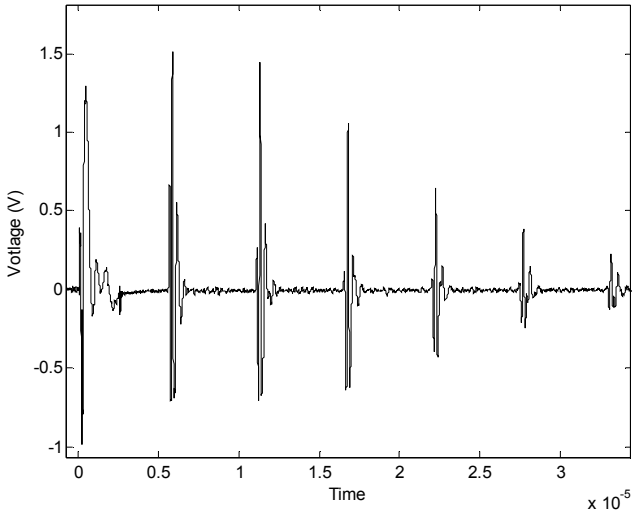

(a)

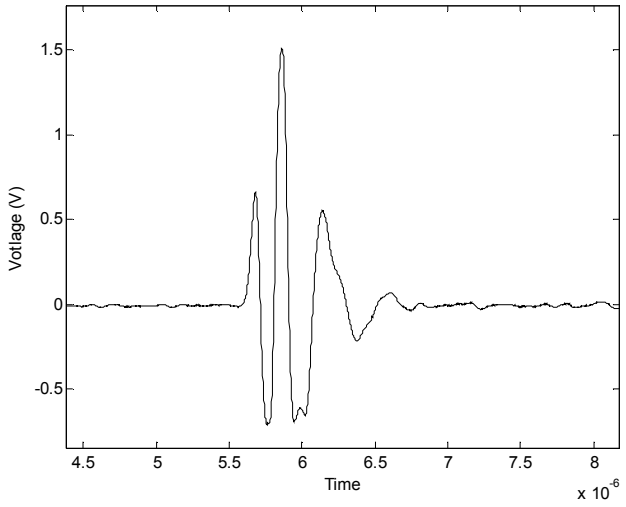

(b)

Fig. 3.6: (a) Signal train and (b) close up of first echo for sample in which the powder/solution were mixed using a high intensity ultrasonic horn.

piece of steel. The sample was sintered in a 2.45 GHz microwave with a multimode cavity at a temperature of about 875 ^{o}C with a 10 min soak time. Gold electrodes 100 nm thick were sputtered onto the sample surface. Fig. 3.6 (a) shows the pulse-echo signal train generated by the transducer and Fig. 3.6 (b) shows a close up of the first echo. This signal had a signal to noise ratio of 64 dB.

3.1.1 Underwater Testing of Longitudinal Wave Transducer

Many applications of ultrasonic transducers require transmission of ultrasonic energy through water and into a sample. Such applications include phased array technology, scanning acoustic microscopy, A, B, and C-scan imaging of structures, as well as examining structures that are submerged in the environments in which they operate. So the next chosen set experiments were chosen to see if these practical applications are feasible.

The first experiment was a through transmission test with a fabricated bismuth titanate samples (deposited onto steel substrates) generating and receiving the signals. The fabrication procedure was the same as the previous sample. One collected waveform is shown in Fig. 3.7. In this experiment the transducers were submerged and placed 20 mm apart from one another. A tone burst excitation signal with a frequency of 2.45 MHz was used.

Next metal bars of different materials and and thicknesses were placed between the transducers to see if ultrasonic energy pass through structures and still be detected.

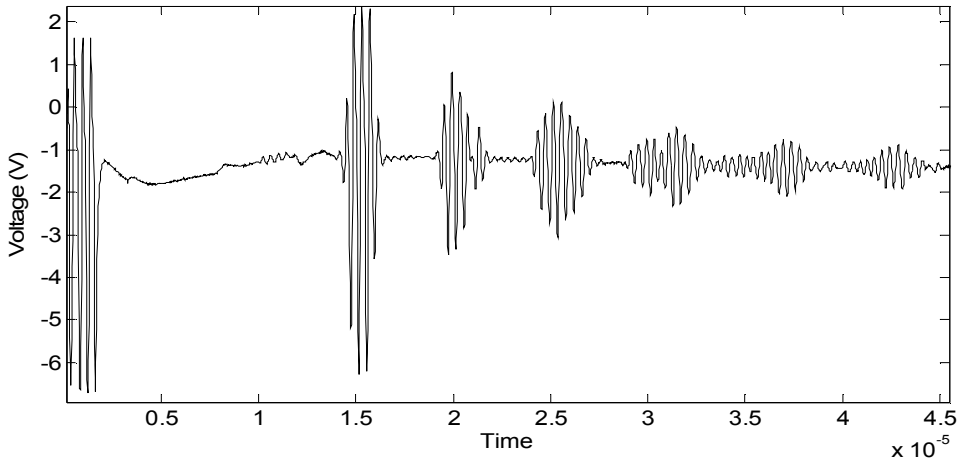

Fig. 3.7: Through transmission of bismuth titanate transducers submerged in water.

Collected wave forms are shown in Fig. 3.8 . In Fig. 3.8 (a), the transducers were 9 cm apart with a 2 mm thick plate of aluminum between them. In Fig. 3.8 (b) the transducers were 20 mm apart with a 3 mm thick zircalloy bar in between them. In Fig. 3.8 (c) the transducers were 30 mm apart with a 7mm thick copper plate placed between them.

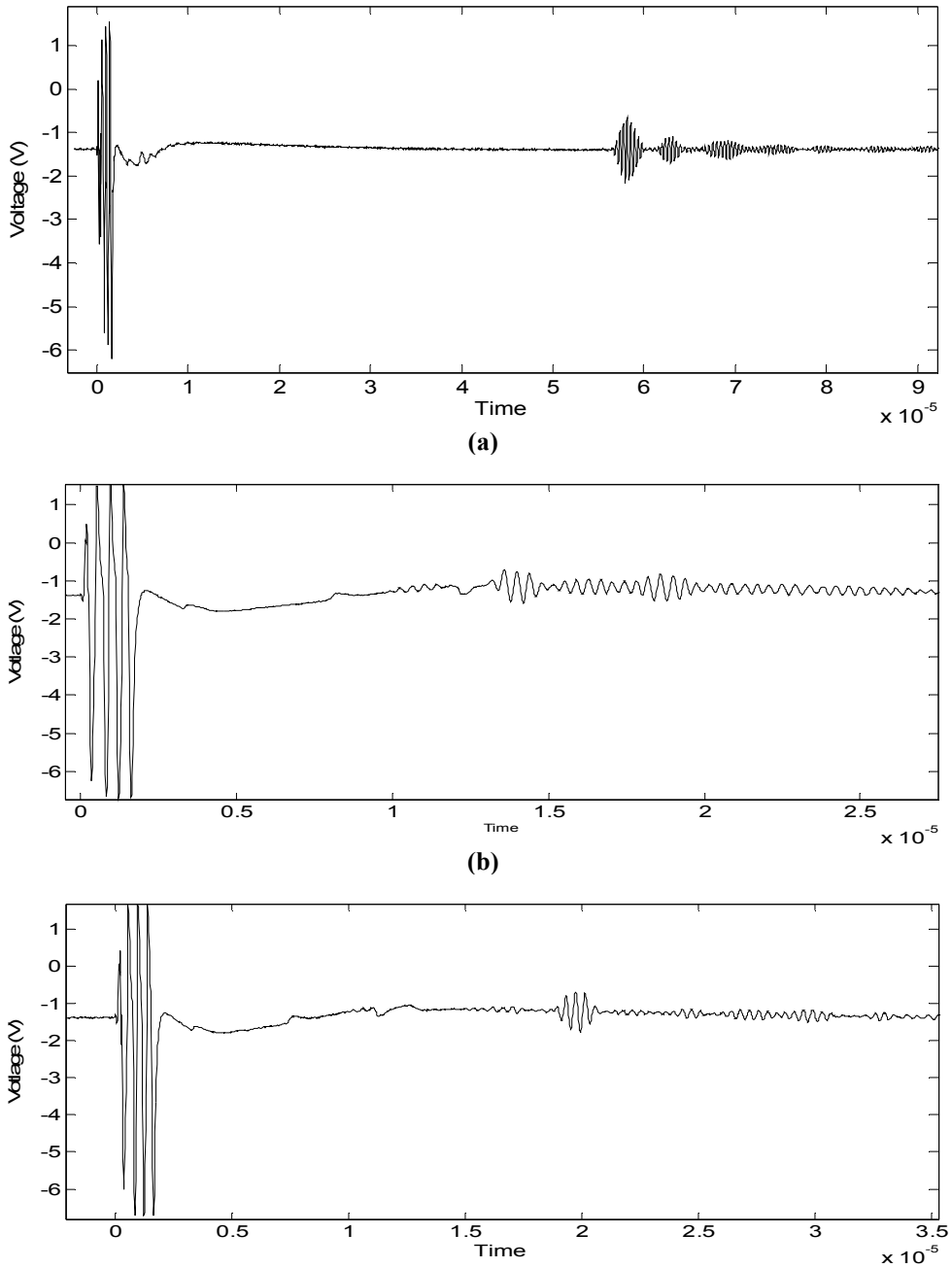

Fig. 3.8: Signals of through transmission through submerged (a) 2mm thick aluminum, (b) 3 mm thick zircalloy, and (c) 7mm thick copper plates.

3.2 Fabrication of Lamb Wave Transducer

Fabrication of transducers for Rayeligh or Lamb wave generation proved to be extremely difficult at first. Samples were first fabricated using the standard chemical powder preperation mentioned in the previous section along with high intensity ultrasonic mixing of the powder/solution. Samples were sintered using a 2.45 GHz mutlimode microwave oven in atomospheric conditions at a termperature of 875 ^{o}C with a soak time of 10 minutes. Samples were poled using both the corona discharge and oil bath poling methods. A shadow mask was used such that interdigitated electrode (IDE) patterns could be deposited on fabricated samples. Interdigital spacing on the patterning was designed with 0.5 mm spacing between the fingers (2 MHz Rayleigh wave on titaniu). An illustration of the IDE pattern that would be deposited after sputtering is shown in Fig. 3.9, the drawing is not to scale and contains a fewer number of finger pairs then the actual pattern. After first being deposited, the electrodes are left shorted such that oil bath poling could be performed over the entire electroded area simultaneously (Fig. 3.9 a). After poling the short would be removed such that the two sides of the IDE pattern would be electrically isolated (Fig. 3.9 b).

Several samples were fabricated with little success. In almost all the samples, despite the electrode pattern, the primary waveform being generated was longitudinal. Therefore if there were any Rayleigh or Lamb waves generated it was almost impossible to tell because they would be buried within the longitudinal backwall reflections. This is suspected to occur because the polarization of bismuth titanate is about an order of

magnitude greater in its ab plane than in the c plane[21]. It has been reported that the polarization along the a-axis is 50 $\mu C/cm^2$ while it is 4 $\mu C/cm^2$ along the c-axis [26].

Another technique that was tried was depositing the bismuth titanate onto thin plates (thickness of the substrate being on the order of or less than the Rayleigh wavelength). It was thought that since the primary vibration mode generated was longitudinal, the boundary conditions imposed by a thin plate would force Lamb waves to form; or, in other words, it was thought that the bottom of the thin plate would force mode conversion of longitudinal waves into Lamb waves. While some waveforms were detected it could not be confirmed that these detected signals were Rayleigh or Lamb waves (e.g. they could not be damped out by appliying pressure to the surface and the waveforms were too complicated to make wave velocity measurements).

In the next attempt a sample was repoled in an oil bath in a different fashion. The aformentioned combined methods of corona and oil bath poling would result such that the bismuth titanate layer's main polarization direction would be out of plane, that is the poling direction would be perpendicular to the electrodes and material surface. It was thought that if the main polarization vector could be aligned in plane, it would increase

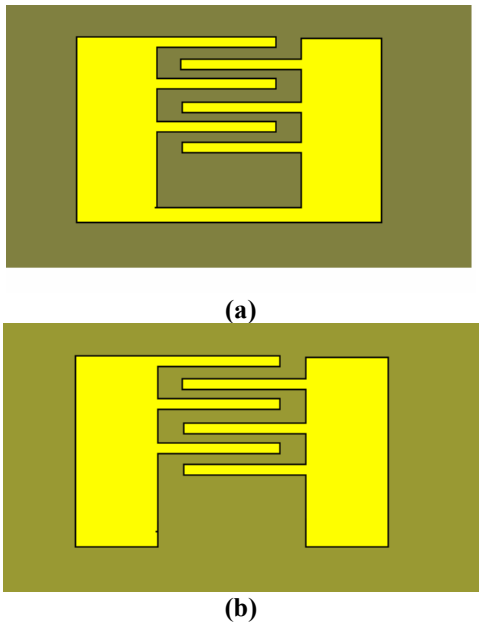

Fig. 3.9: Deposited electrode orientation (a) prior to and during poling and (b) for use to generate Lamb or Rayleigh waves after poling.

the chances of creating a Rayleigh or Lamb wave.

To accomplish this psuedo in-plane poling, the sample was again corona poled so that there would be a net alignment or polarization vectors out of-plane. Next the gold electrodes were sputtered on in the pattern of Fig. 3.9 (a). Prior to oil bath poling, the short between the electrodes was removed such that the pattern looked like Fig. 3.9 (b). During oil bath poling one side of the electrode pair was connected to high voltage positive terminal and the other side was grounded (Fig. 3.10 (a)). It is thought that electric field within the material would give a pseudo in-plane poling. Fig. 3.10 (b) demonstrates what the suspected internal electric field lines during poling would like in a cross section of the material. In Fig. 3.10 (b) not all the field lines have drawn (e.g. lines between one pair of negative and positive electrodes have been omitted for

simplification) and some field lines would be expected to be out of plane; going from the electrodes down to the

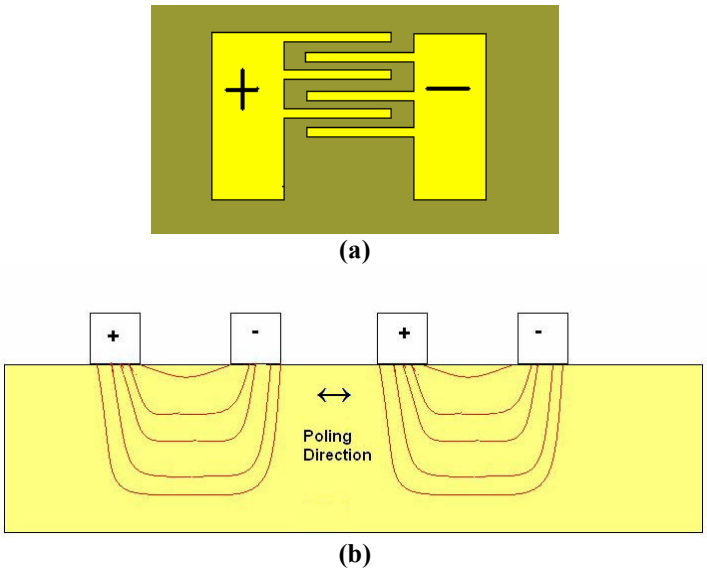

Fig. 3.10 (a) Electrode polarity during poling and (b) simple schematic of electric field line orientation within the material during poling.

metallic substrate, especially at points directly beneath the positive electrodes.

The first sample this poling technique was attempted had a thin stainless steel plate substrate that with a thickness of 1.55 mm. The distance from the front most IDE finger to the plate edge was 16 mm, the distance from the backmost IDE finger was 18 mm; the plate had a width of about 30 mm and a length 50.75 mm. These dimensions are shown in Fig. 3.11. The sample was poled using the above in-plane poling technique at a voltage of about 600 V (voltages any higher were causing electrical breakdown).

The first detected signal to be confirmed as a Lamb wave is shown in Fig. 3.12 (a). The excitation signal was 3.08 μs tone burst with a frequency of 2 MHz (plate thickness is 1.5 mm, giving an fd product of 3). The signal was filtered using a band pass

filter that allowed frequencies between 1 and 10 MHz. A gain of 56 dB was used. The waveform was easily damped by applying pressure to the plate surface; this indicates out of plane displacement on the plate surfaces. A comparison of damped and undamped signals is shown in Fig. 3.12 (b).

Further proof that out of plane surface displacements were occurring was obtained by taking displacement measurements using a Laser Doppler Vibrometer. These results are shown in Fig. 3.13 ; the y-axis of the graph is displacement in nm. In the experiment, the laser beam was focused on a spot 13 mm away from the closest IDE finger. From the plot it appears that the first detected signal is arriving at 5.264 μs. This would give the wave a velocity of almost 2.5 μs. This velocity doesn't correspond to the arrival times seen in Fig. 3.12. There, the first train arrives at 6.7 μs and the second major train arrives at 27.5 μs; these would correspond to wave velocities of 4.85 mm/ μs and 3.05 mm/ μs.

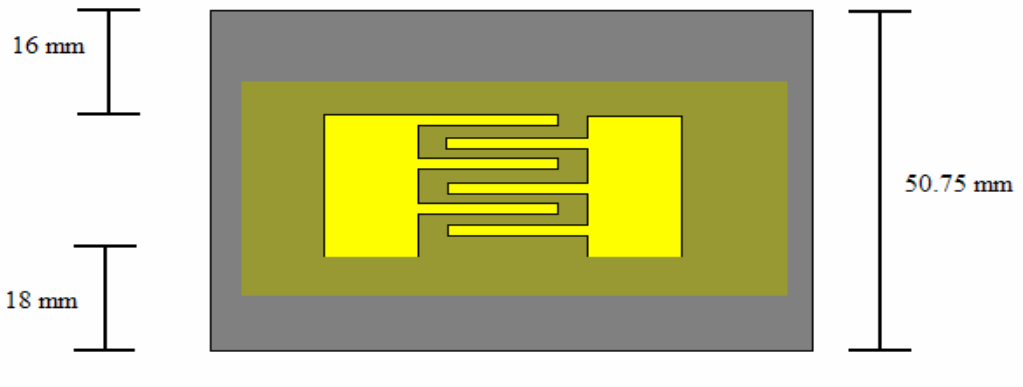

Fig. 3.11: Dimensions of sample to first generate Lamb waves.

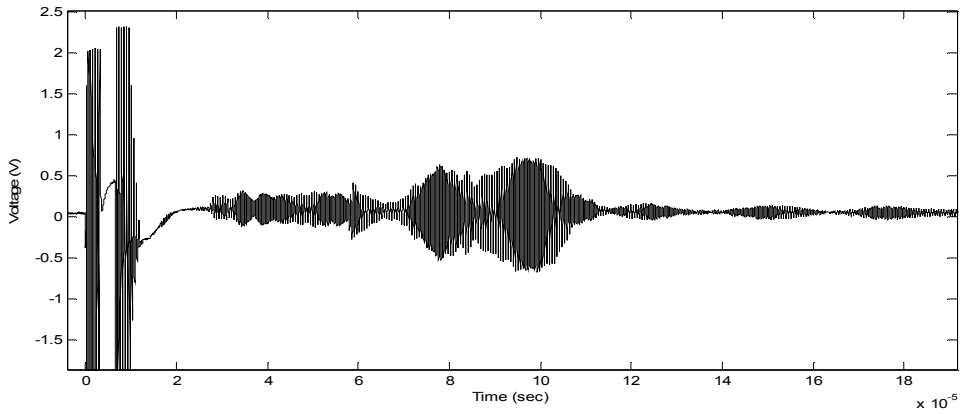

(a)

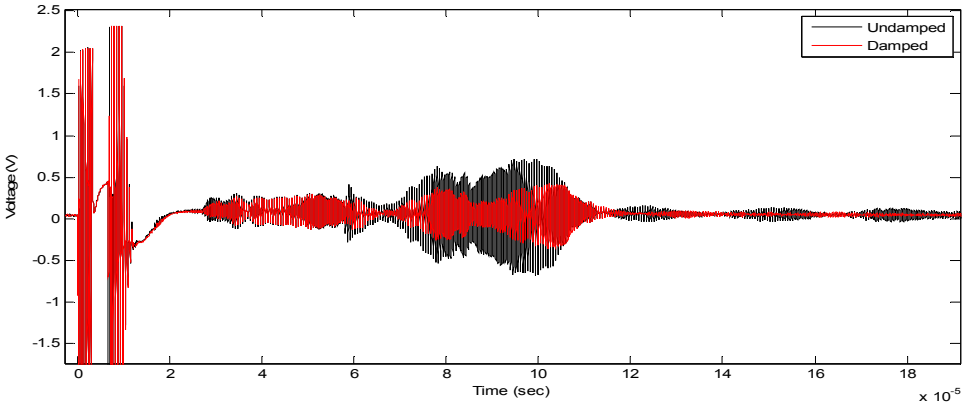

(b)

Fig. 3.12: (a) Damped and (b) comparison of damped and undamped Lamb wave signals.

However the LDV is detecting only out of plane displacements and also the fact that with the laser beam only 13 mm away from the IDE all the wave packets of the different vibration modes more than likely haven't yet fully developed yet.

3.3 Rayleigh Wave Generation

Attempts at creating Rayleigh waves in the plate sample described above were difficult. The plate thickness, 1.5 mm, is on the order of the dimensions of the

wavelength of a Rayleigh wave at the designed frequency of 2MHz. Therefore it is possible that there could be Rayleigh waves in the echograms along with the detected Lamb waves but this is almost impossible to determine. One approach to test for Rayleigh waves would be to fabricate a new sample on a thicker and longer metallic substrate; but this requires the use of larger sputtering chambers for the deposition of electrodes which can be costly. As a result a different approach was undertaken to test the feasibility of Rayleigh wave generation using bismuth titanate.

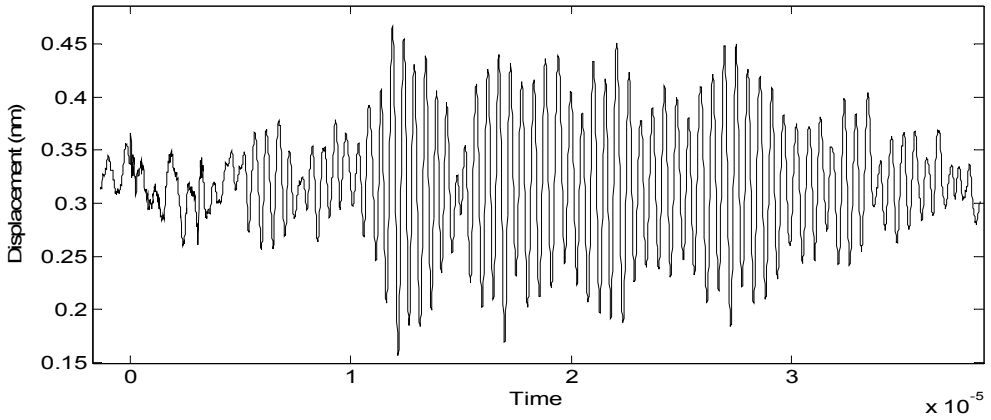

Fig. 3.13: Laser Doppler Vibrometer displacement measurements.

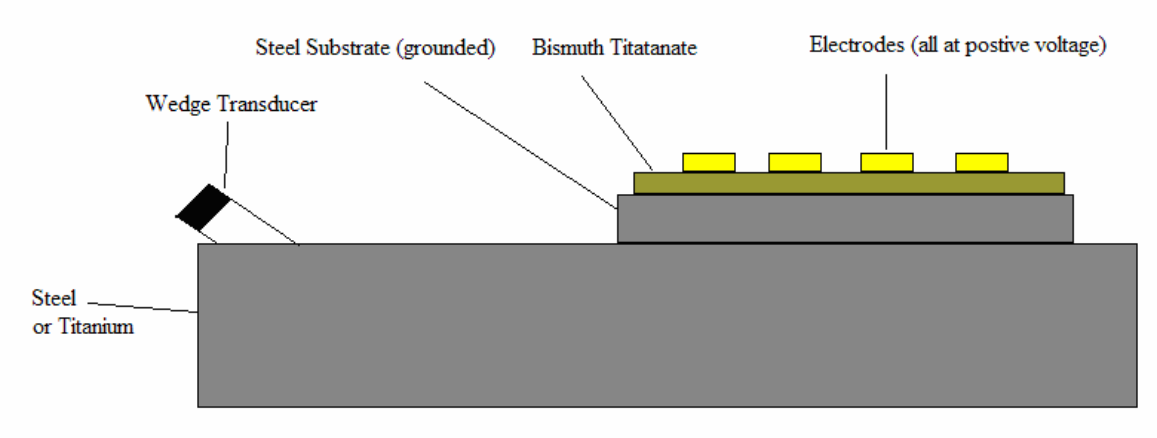

Fig. 3.14: Experimental setup for Rayleigh wave generation.

In this approach, the plate sample used in 3.2 was again utilized. This time the electrodes on the sample were left shorted as is shown in Fig. 3.9 (a). The sample was placed on top of a thicker and longer metallic specimen with a thin layer of gel between the two to serve as a mechanical couplant. Located at a distance away from the plate sample was a 2.25 MHz commercial transducer on top of 70^{o} wedge (which is, for most metals, well beyond the second critical angle that is discussed in Eq. 1.18). The experimental setup is illustrated in Fig. 3.14.

The first surface the sample was placed onto was a titanium bar was 6.4 mm thick. A tone burst excitation with a frequency of 2.2 MHz and a pulse width of 7.94 μs. For titanium, c_R = 2.79 mm/μs therefore at 2.2 MHz the Rayleigh wavelength was 1.27 mm. Since the bar is over 6 mm thick there should predominantly be Rayleigh waves. Signals obtain from the commercial receiving transducer at distances 138mm and 183 mm away from the leading edge of the electrodes are shown in Fig. 3.15. At these distances the signal arrival time for a Rayleigh wave can be calculated to be 49.4 and 65.6 μs. In the experiment, the arrival times for the distances of 138 mm and 183 mm

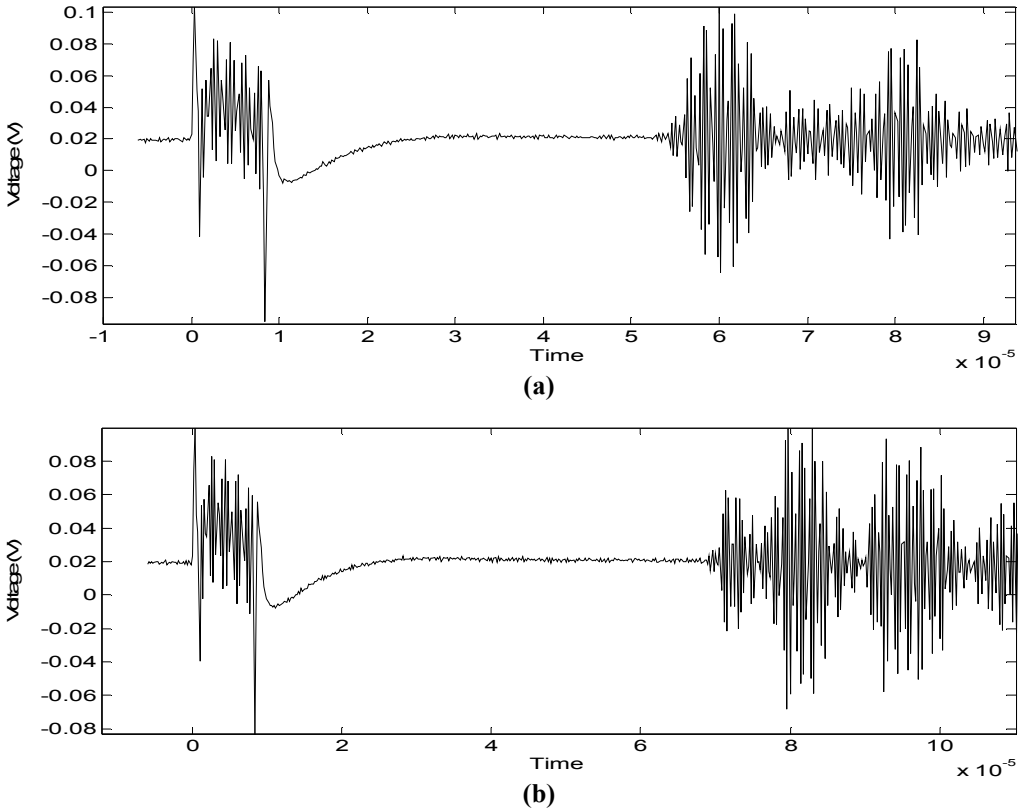

Fig. 3.15: Signals received from commercial transdancuer located at distances (a) 138 mm and (b) 183 mm away from bismuth titanate plate sample.

are 52.4 μs and 69 μs which agrees well with the calculated values. In all cases applying pressure to the bar between the sample and the wedge transducer caused significant signal damping.

In the waveforms of Fig. 3.15 there is a significant amount of ultrasonic energy following the arrival of the first signal. These later wave packets are believed to be from reflections of waves trapped within the substrate escaping after multiple reflections. These waveforms may also be longitudinal/shear waves being sent into the titanium bar and are then mode converting and reflecting once they hit the front and back walls of the titanium bar.

Next the sample was tested to see if Rayleigh waves could be seen in pulse-echo mode. One of collected waveforms is shown in Fig. 3.16. In this case the bar end was located 196 mm away from the leading electrode edge; this would correspond to a Rayleigh wave arrival time of about 140.5 μs. However there is significant signal content throughout the entire time, presumably from Lamb wave reflections traveling within the substate as well as reflections from longitudinal and shear wave traversing the thickness of the titanium bar. Attempted damping of the signal by applying surface pressure also provided no conclusive evidence. It is suspected that the sharp boundary located at the edge of the sample steel substrate may make it difficult for a Rayleigh to enter back into the substrate and then reach the bismuth titanate. Therefore the evidence seen thus far shows no convincing evidence of having seen Rayleigh waves while operating in pulse-echo mode.

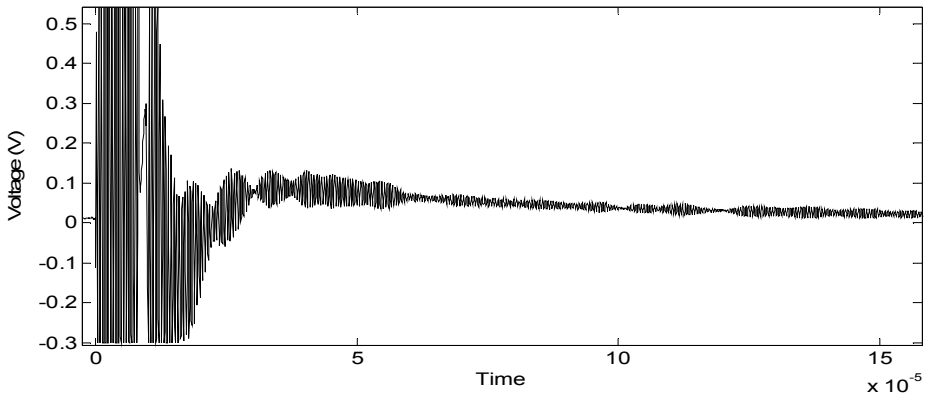

Fig. 3.16: Detected signal in pulse echo mode.

Chapter 4

Performance as a Transducer at High Temperatures

4.1 High Temperature Experimental Setup for Longitudinal Vibration Transducer

The first transducer to be tested at elevated temperatures was a longitudinal mode transducer 1.35 cm thick, sintered at 850 ^{o}C for ten minutes in multimode microwave chamber at 2.45 GHz with HIU treatment of the solution/powder with gold electrodes. The sample was corona poled and later oil bath poled. During the experiment the samples electroded area was 3.4 cm^2.

The goal of the experiment was to operate the transducer in pulse-echo mode and raise the temperature until the transducer ceased to be operational. As it was mentioned in Chapter 1, bismuth titanate has a Curie-Weiss temperature of 685 ^{o}C and therefore it was assumed that the transducer would be operating at temperatures exceeding melting points of most common solders so a special experimental setup had to be devised.

Common BNC cables would not be able to withstand the high temperatures so it was known that wires (uninsulated) having high melting temperatures would have to be fed into the oven to the transducer from the outside. The wire leads would be connected to the signal source by using alligator clips connected from a BNC cable. It was decided that the best way to ensure electrical connectivity between the wires and the transducers electrodes would simply be through mechanical contact. The wire leads would be

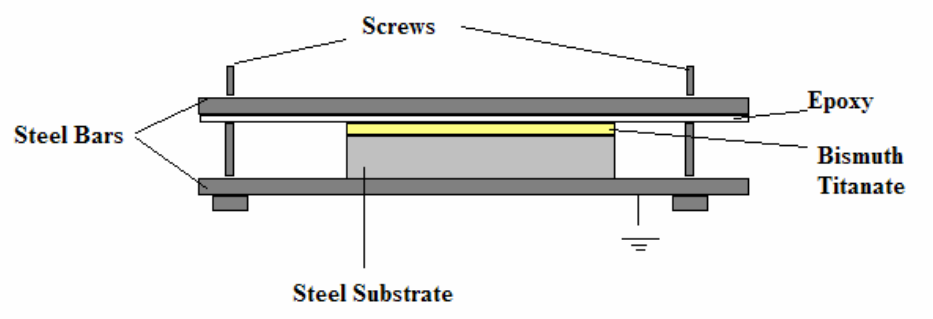

Fig. 4.1: Schematic of sample holder for high temperature experiments..

forcibly held in contact to the electroded surface (positive) and the samples steel substrate which would act as the ground.

To ensure a mechanical contact that would secure electrical connectivity throughout the experiment a holder that is shown schematically in Fig. 4.1 was constructed. The apparatus consisted of two steel bars that could be tightened on one another by two steel screws with nuts on their bottom ends. One steel bar was coated with a high temperature ceramic epoxy. The bismuth titanate sample was placed in between the two the bars. The positive wire lead was run between the bismuth titanate's electroded surface and the epoxy coated steel bar. Screws were run between the bottom uncoated bar and epoxy coated bar and tightened with nuts. The rest of the holder was put to ground. The epoxy coated surface would ensure mechanically that electrical connectivity would be maintained while at the same time maintaining isolation between the positive wire and the grounded sample holder. The apparatus was also designed with the idea that as the holder thermally expanded the nuts on the screws would also expand, preventing the screws from loosening and therefore keeping the two bars tightly held to the sample.

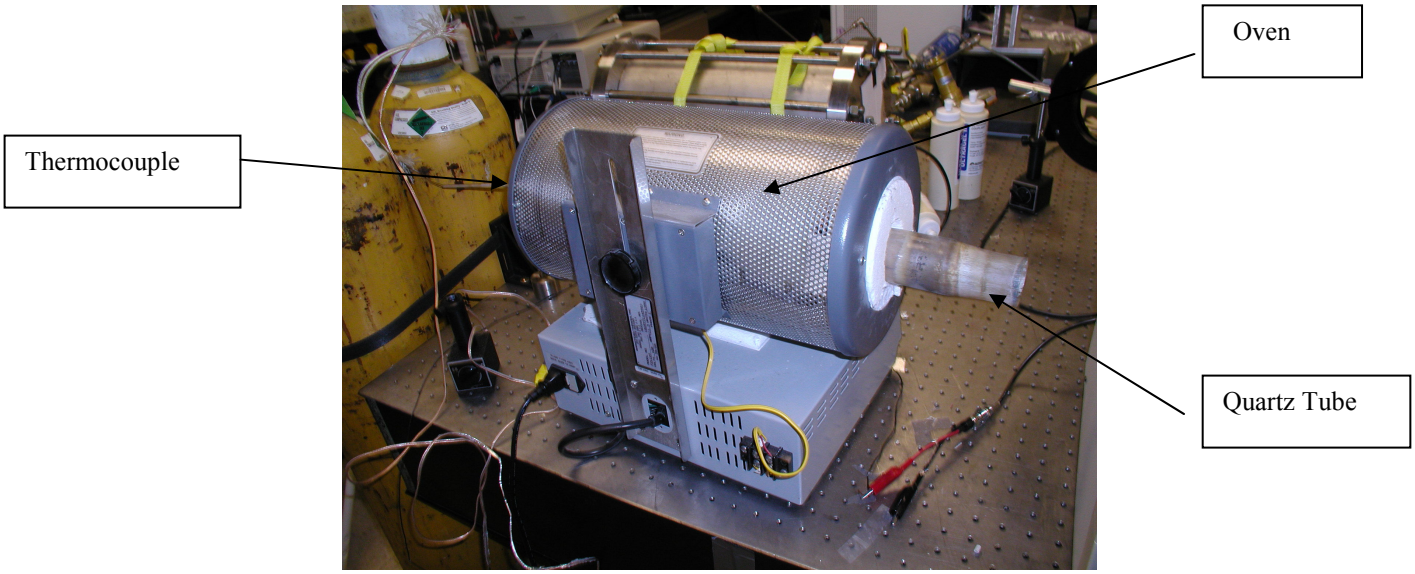

Fig. 4.2: Oven setup for high temperature experiments.

The oven used to heat the sample was a Thermolyne tube furnace. The tube running through the furnace was made of Quartz and would help to ensure thermal equilibrium inside the furnace. The tube was closed at both ends except for small holes where the electrical leads and thermocouple would be fed in at. The thermocouple used to measure temperature was an Omega K-type thermocouple connected to an Omega HH81 digital readout. A ceramic cylinder with a divider in the middle would ensure that the thermocouple leads would remain electrically isolated from one another. The oven setup is shown in Fig**. 4.2.**

4.2 High Temperature Testing of Longitudinal Wave Transducer

For the experiment to test the sample ultrasonic performance at high temperature the excitation signal used was a 3.1 MHz tone burst with a pulse width of 0.82 μs . A tone

burst signal was used so that the signals frequency could be optimized for maximum transducer output and also it was assumed that there would be much less noise by using a lower frequency tone burst than there would be if a high frequency pulse were used. The received signal was filtered using a band pass filter with the high and low pass frequencies at 1 MHz and 5 MHz, respectively. The received signal had a 55 dB gain. A plot of measured temperature and time during the experiment is shown in Fig. 4.3. The average heating rate during the experiment was held low to an average 1.5 ^{o}C/min to ensure thermal equilibrium between the sample and environment. The waveform recorded at room temperature is shown in Fig. 4.4**;** Fig. 4.4 (b) shows a close up of the first echo which is compared in subsequent echographs taken at higher temperatures. The signals in Fig. 4.4 contain a higher noise level than the signals in Chapter 3. This is attributed to the fact that long, unshielded wires (~ 1 m) had to be used in order to reach the transducer inside the oven. Since the operating frequency was 3 MHz it is understandable that there is some noise infiltrating the signal.

Fig. 4.5 and Fig. 4.6 show signals obtained over the temperature range 23 – 681^{o}C. Up until about 550 ^{o}C the signals lost little or no amplitude. Shifts in arrival time are present most likely due to the elastic wave speed changing due to changes in the steel's mechanical properties. After 550 ^{o}C the signals amplitude began to decrease rapidly. By 681 ^{o}C the signal was completely lost. No ultrasonic waves could be generated from the transducer after the sample cooled; this confirmed that the sample had become completely depolarized.

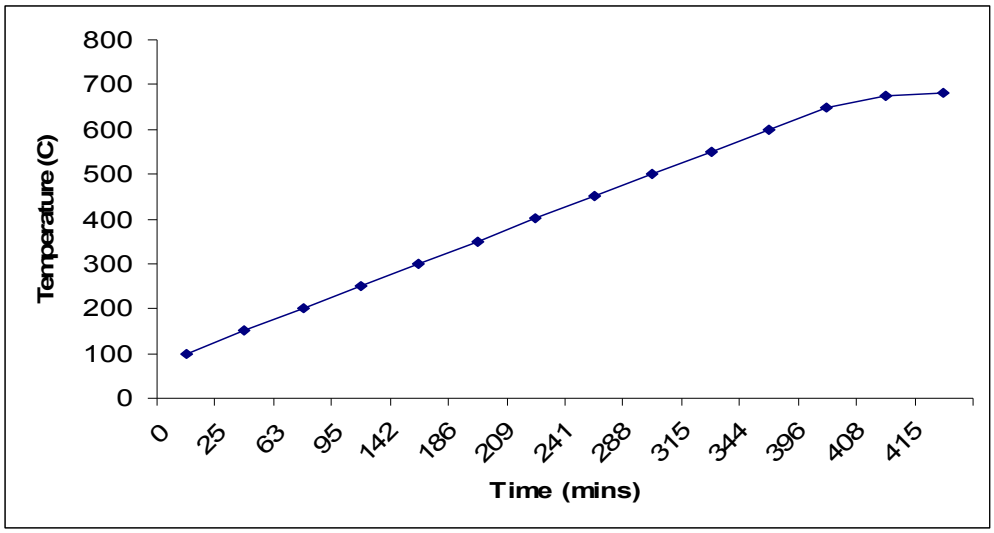

4.3: Heating rate during testing of longitudinal vibration transducer.

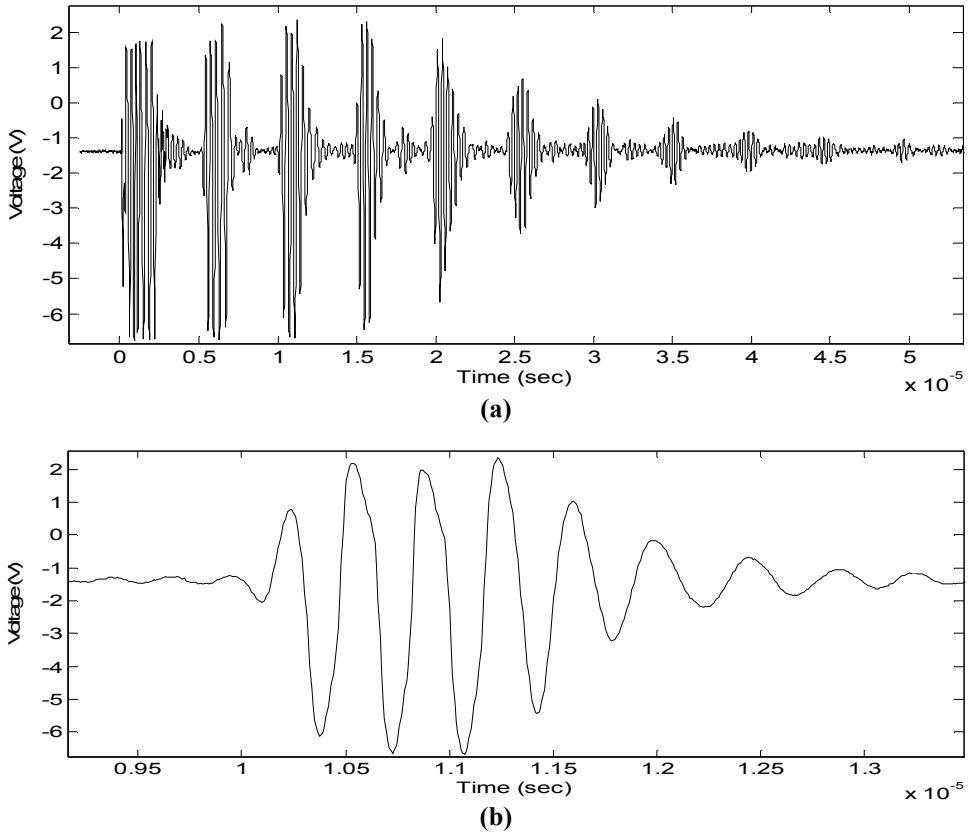

Fig. 4.4: (a) Signal train recorded at room temperature and (b) close up of the first echo.

It was unexpected that the sample would be able to achieve operating temperatures up to 680 ^{o}C. It was thought that the sample would lose its efficiency and would no longer be able to generate ultrasonic waves by about 550-600 ^{o}C. Therefore, to ensure that the transducer and the environment were in thermal equilibrium and to see if the transducer could maintain operation at elevated temperatures the sample was repoled and, using the same experimental setup, the transducer was tested for an extended period of time at 600 ^{o}C. The sample was held at this temperature for over an hour and maintained its efficiency. The temperature was raised further to 625 ^{o}C and was held there for 3 hours with the sample maintaining ultrasonic functionality. The waveforms from this second experiment are shown in Fig. 4.7. Therefore this experiment confirmed that the sample was able to maintain ultrasonic wave generation at these temperatures for at least brief periods of time. It should also be noted that the samples efficiency was reduced from the first experiment (e.g. signal amplitudes were much smaller). This is attributed to the fact that the sample was much more difficult to pole (electrical breakdown was occurring at 500 V). The cause of this isn't exactly known, but it is thought that during the temperature experiment grains within the bismuth titanate grew from exposure to the high temperatures for long times. Previously reported work by Shulman indicate that conductivity in bismuth titanate is through the grains, this would lead to an increase in material conductivity and then would result in difficulty repoling the sample [21].

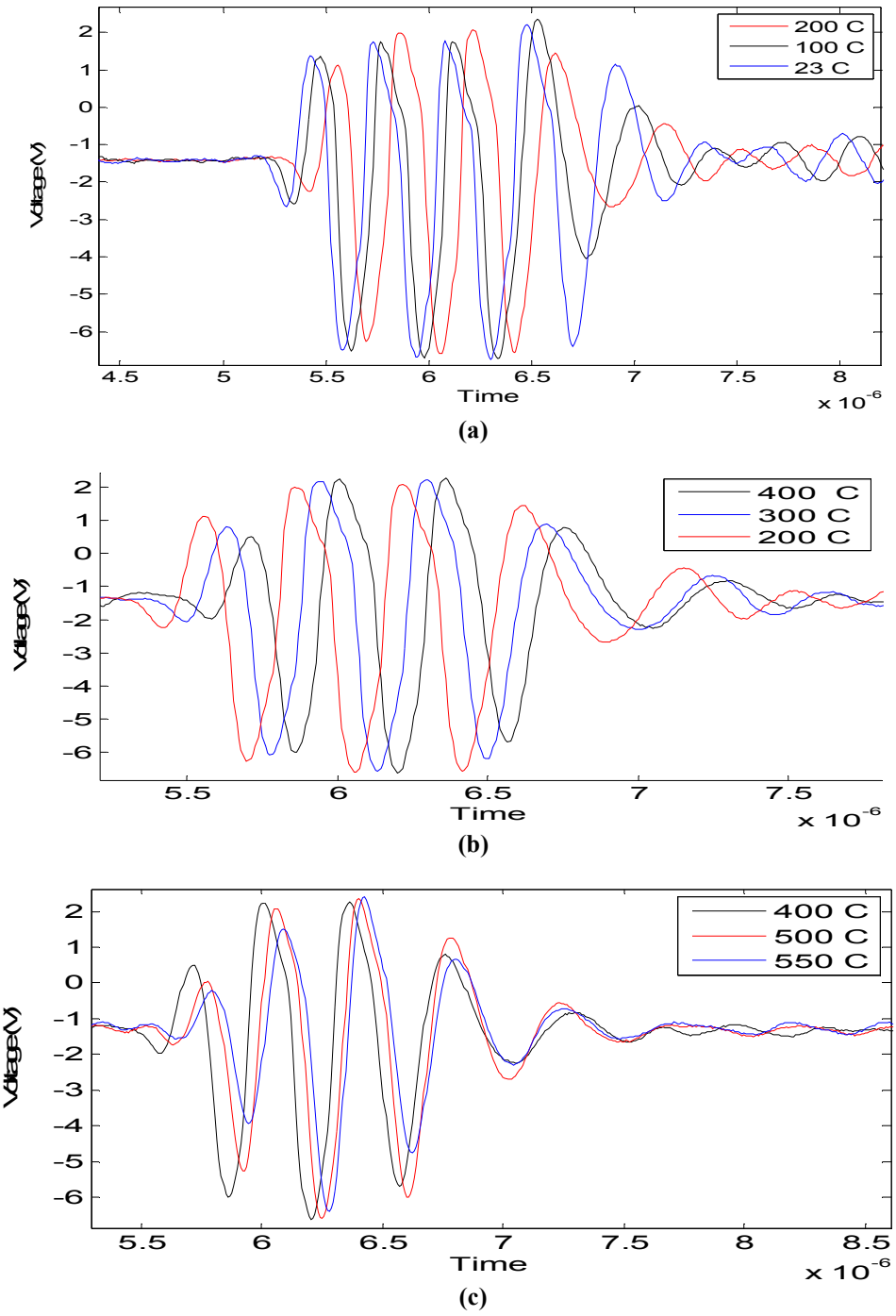

Fig. 4.5: Received signals at temperatures (a) 23 - 100 ^{o}C, (b) 200 - 400 ^{o}C and (c) 400 - 500 ^{o}C.

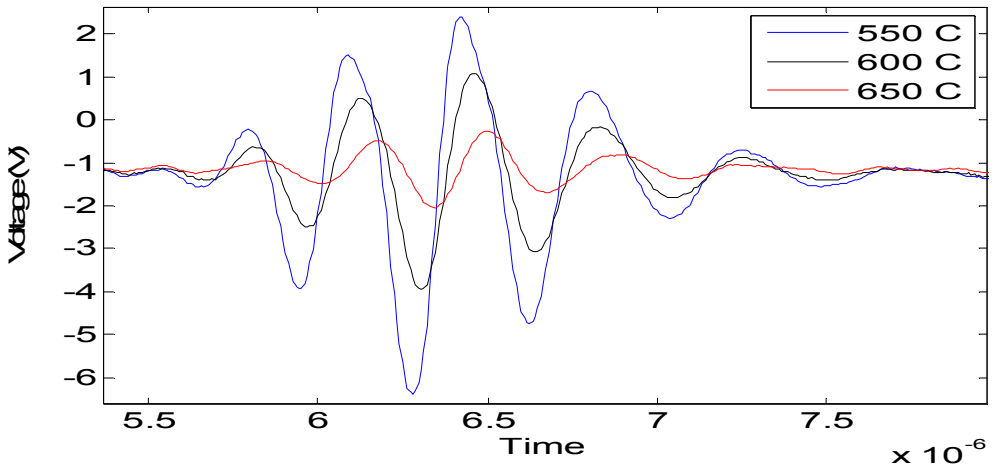

(a)

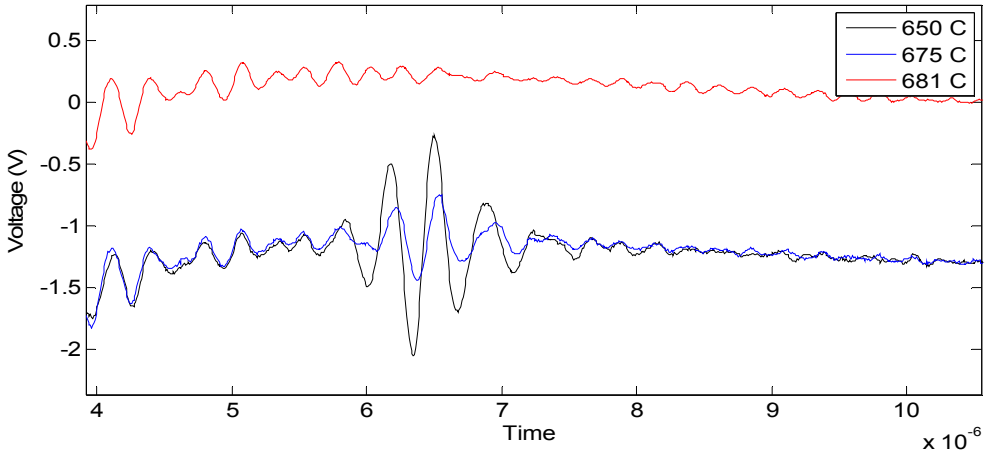

(b)

Fig. 4.6: Signals at temperatures (a) 550 – 650 ^{o}C and (b) 650 – 681 ^{o}C.

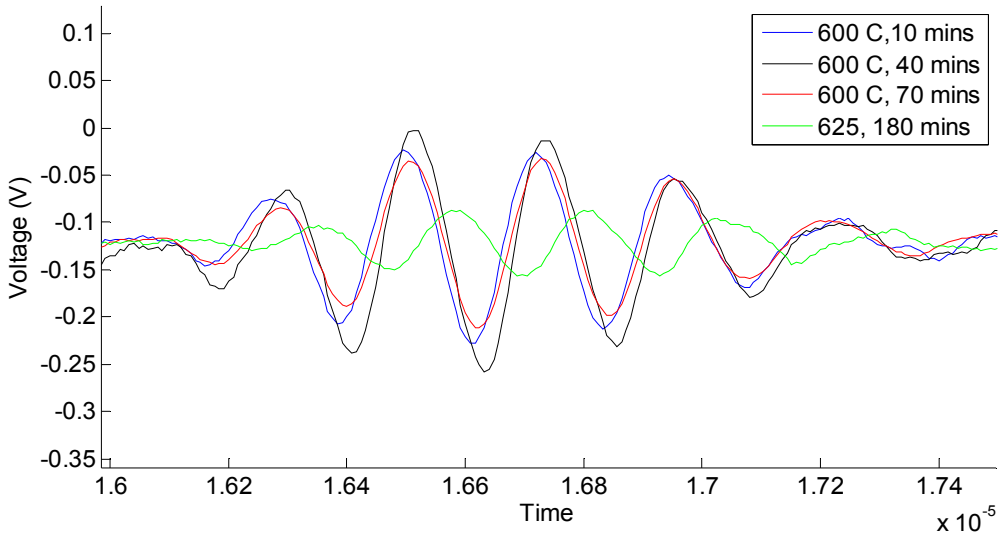

Fig. 4.7: Signals obtained for bismuth titanate transducer held at 600 ^{o}C and 625 ^{o}C for over one hour and 3 hours, respectively.

4.3 High Temperature Testing of Lamb Wave Transducer

To test the performance of the Lamb wave transducer described in Chapter 4.2, a similar experimental setup that is described in Chapter 4.1 was created and is described briefly here. Again, a two bar apparatus was built with one end coated with a high temperature epoxy. However, for this experiment more care had to be taken to make sure that most of the surface of the transducer was not in contact with any other surface to prevent damping of the signals out of plane vibrations. A schematic of the apparatus built for the experiment is shown in Fig. 4.8. Again epoxy coated steel would be used to hold the positive leads mechanically onto the electrodes; however in this setup small pieces were connected to the main steel bar such that surface area of the transducer in contact with another material was minimized. The bottom of the steel substrate would rest on two

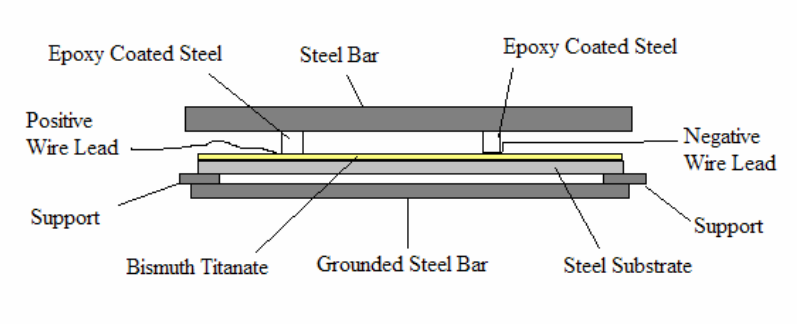

Fig. 4.8: Experimental setup for high temperature testing of Lamb Wave Transducer.

steel supports which came in contact only on its sides. The supports themselves were joined to the main bottom bar which was grounded. Again, screws with nuts attached to the end were used to hold the apparatus together tightly. The screws are not shown in Fig. 4.8 to keep the schematic from becoming to complicated to view.

Temperature as a function of time for the experiment is plotted in Fig. 4.9. The average heating rate for the experiment was about 1 ^{o}C/min. During the experiment a tone burst excitation was again used. The frequency was 1.9 MHz with a pulse width of 3.06 μs. The original gain was at 55 dB, but had to be lowered as the experiment went on to eliminate noise that became larger as the temperature increased (this is seen as a bend in the signal). A band pass filter allowing frequencies between 1-2.25 MHz was used.

The entire waveform collected at 22 ^{o}C is shown in Fig. 4.10. Close attention will be paid to the waves arriving between 20 μs and 90 μs because, as it was shown in Chapter 4.2, that between these times Lamb waves were being received in pulse echo mode. It was also demonstrated prior to the experiment that these waveforms could be damped out by putting pressure on the top surface; indicating an out of plane displacement. Waveforms collected at temperatures between 22 ^{o}C and 200 ^{o}C can be found in Fig. 4.121. Waveforms collected between the temperatures 455 ^{o}C and 617 ^{o}C

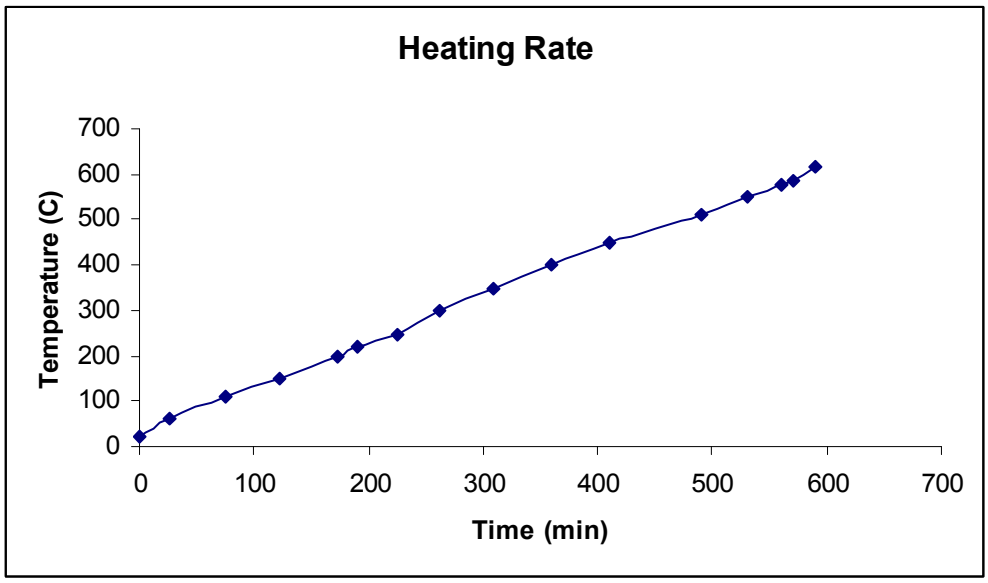

Fig. 4.9: Temperature versus time for Lamb wave sensor high temperature experiment.

are shown in Fig. 4.13.

The recorded waveforms show that the wavelet shape is very sensitive to slight changes in temperature. Changes in the wavelet shape are already observable in Fig. 4.12 (a) where the temperature change is only from 22 ^{o}C to 60^{o} C. This point is demonstrated further in Fig. 4.12 where waveforms collected at 22 ^{o}C and 200 ^{o}C are compared. This indicates that the dispersive properties of the system, or more precisely the phase and group velocities, are also very sensitive to changes in temperature of the system. This is to be expected because not only are the physical material properties

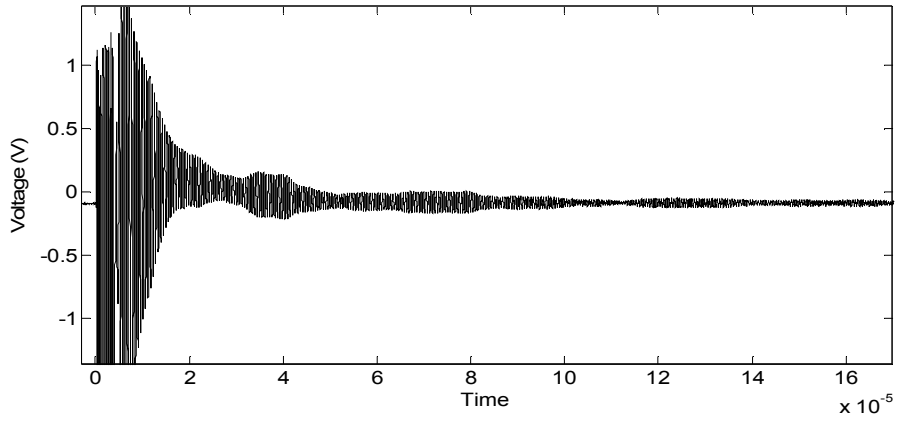

Fig. 4.10: Room temperature wave form.

changing with temperature but so are the dimensions of the system. However, the priority of this work was to study the maximum temperature this system can operate at and close physical explanation of changes in the systems dispersive behavior have been left for future work.

Although in this case it is more difficult to tell because of systems dispersion, the transducer efficiency seems to be temperature independent up until about 400 ^{o} C. After this temperature the overall amplitude of the wavelets begin to decrease. By 575 ^{o}C most of signal has disappeared and just after 617 ^{o}C the signal died out completely. The max temperature for this system is about 65 ^{o}C lower than what was observed for the longitudinal wave transducer in 4.2. This result was anticipated because Lamb waves require both transverse and longitudinal components. Since the polarization in the c-axis of bismuth titanate is almost an order of magnitude lower than that of the a-axis, it was expected that the wave generation/reception associated with this plane would die at a lesser temperature along with the signal associated with Lamb waves.

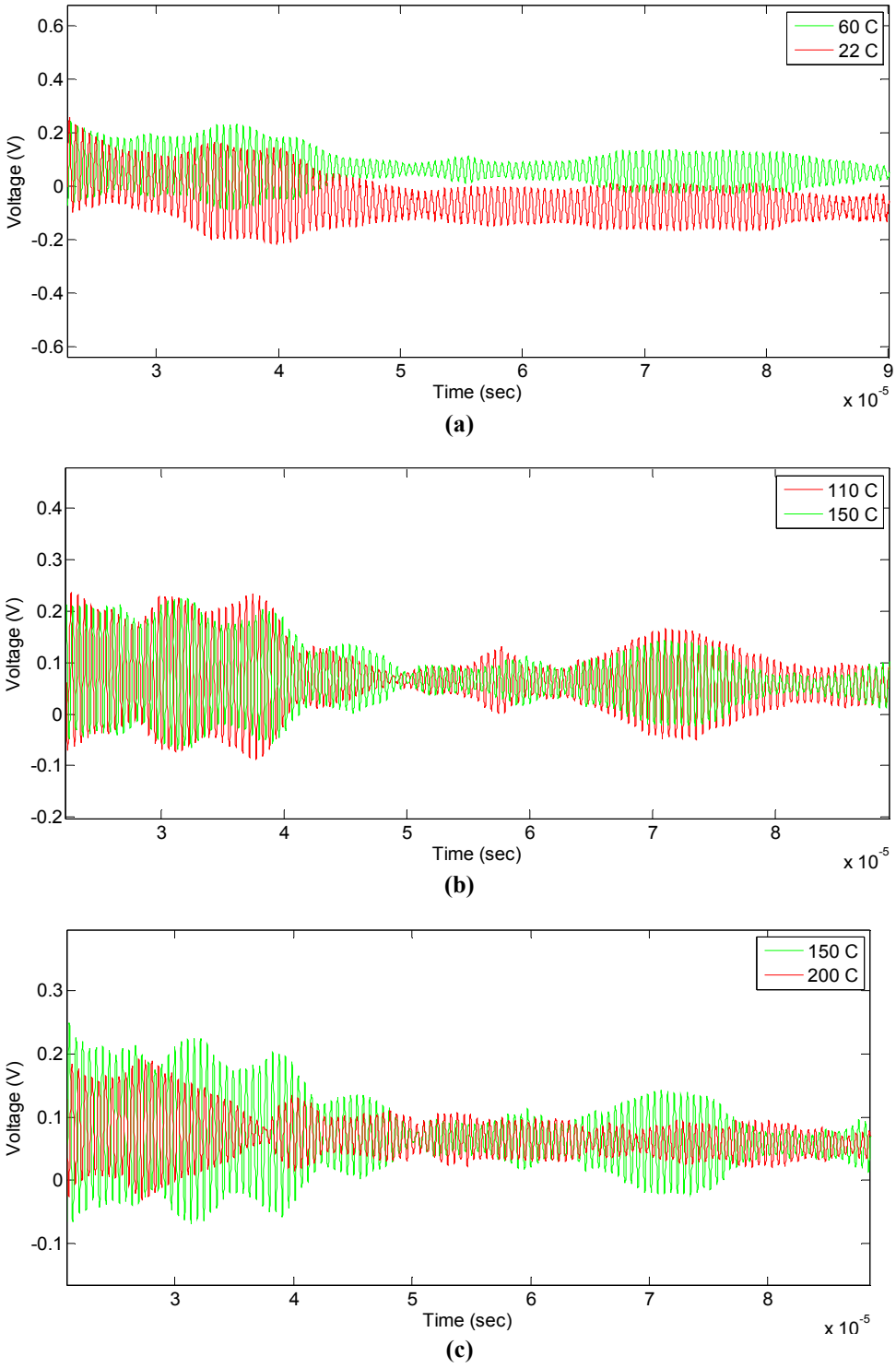

Fig. 4.11: Lamb wave transducer signals received at temperatures (a) 22 ^{o}C and 60 ^{o}C, (b) 110 ^{o}C and 150 ^{o}C and (c) 150 ^{o}C and 200 ^{o}C.

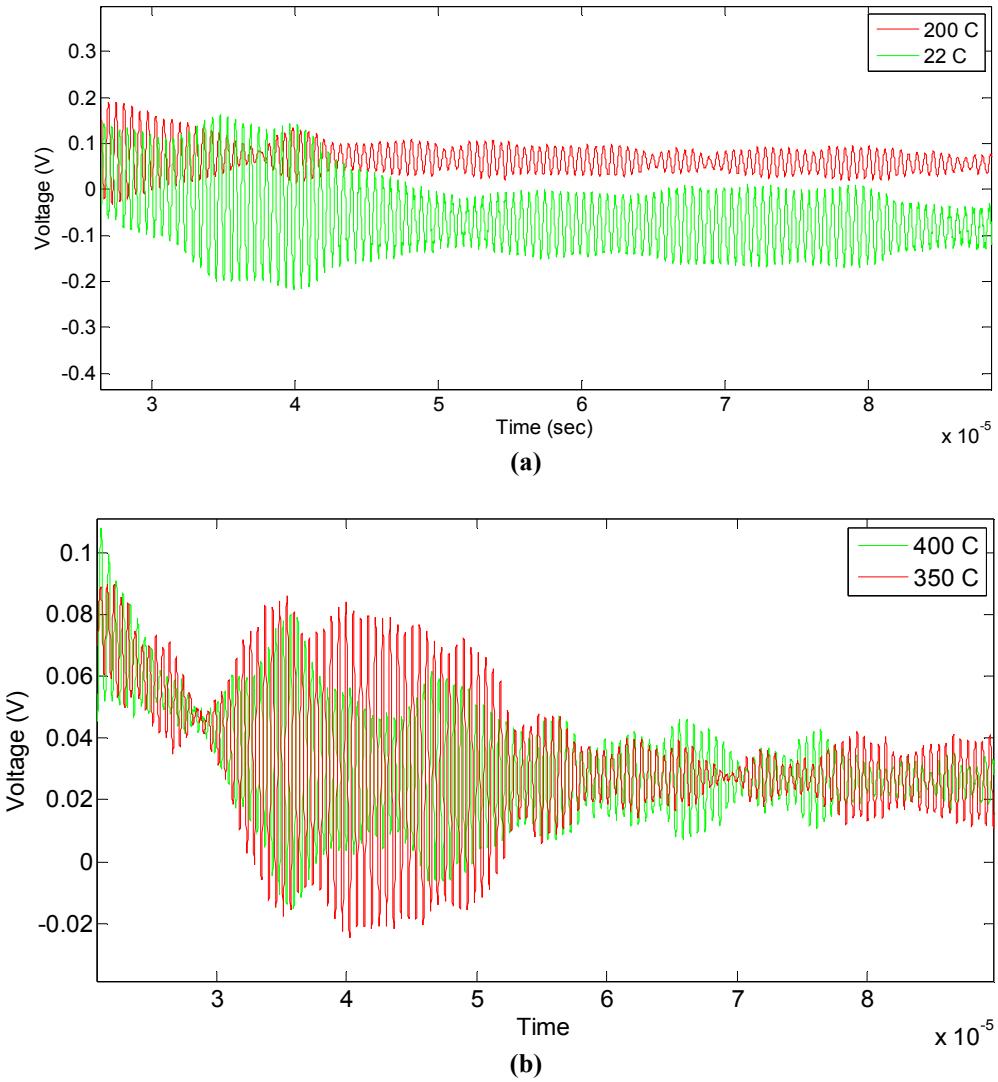

Fig. 4.12: Comparison of waveforms collected at (a) 22 ^{o}C and 200 ^{o}C.and (b) 350 ^{o}C and 400 ^{o}C.

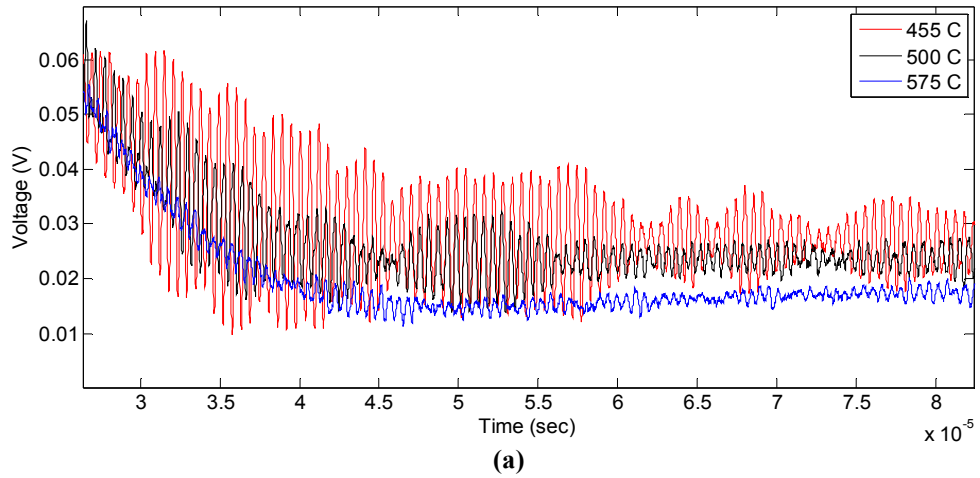

(a)

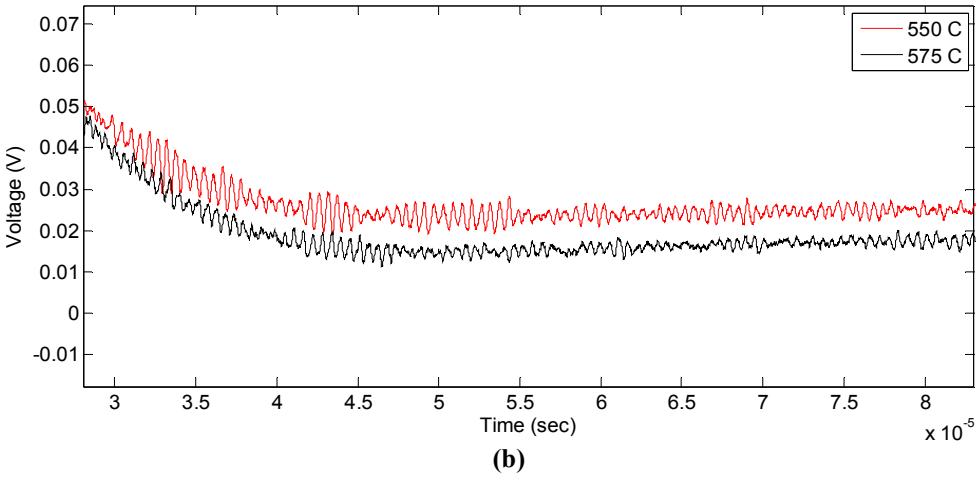

(b)

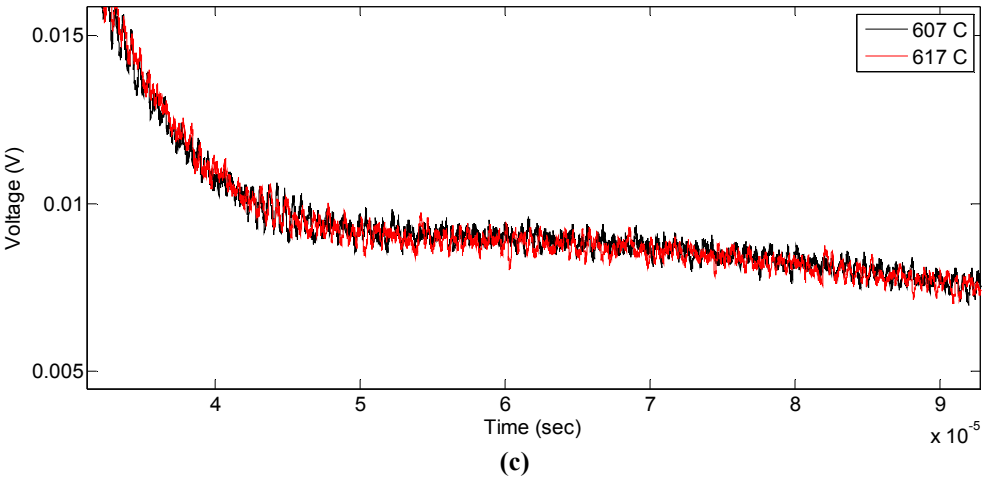

(c)

Fig. 4.13: Waveforms collected at temperatures (a) 455 ^{o}C, 500 ^{o}C and 575 ^{o}C, (b) 550 ^{o}C and 575 ^{o}C and (c) 607 ^{o}C and 616 ^{o}C.

Chapter 5

Summary

5.1 Conclusions

The sol-gel technique described in [27-29] has been adapted and employed. Comparing performances of samples fabricated using different techniques indicate that microwave sinterning in combination with high intensity ultrasound as a substitute for ball milling produce the best transducers. Microwave sintering improved material adhesion, sensor efficiency, and reduced fabrication times. High intensity ultrasound has been incorporated as a substitute for ball milling to avoid contamination and also has reduced time necessary to fabicate samples. The poling process was also further modified by complimenting the corona poling technique with oil bath poling after electrodes have been deposited.

It has been shown that bismuth titanate can serve as a material for longitudinal, Lamb, and Rayleigh wave (through-transmission) transducers. The transducers demonstrated strong preference to generate waves in direction of the materials strongest polarization axis. In order to achieve Lamb wave vibrations in a plate, an in-plane poling technique of the material had to be used. It is also necessary that the electrodes have low resistivity. It has been shown that it is possible to generate longitudinal waves up until a temperature of 680 ^{o}C. Likewise, it has been shown that Lamb wave generation is possible to 617 ^{o}C.

5.2 Recommendations for Future Work

Several areas require further investigation and they are mentioned as follows.

1. **Investigate effects of sintering times and temperatures**

The most successful transducers in this work were sintered at a temperature of 875 ^{o}C for 10 minutes. Since grain size is a function of sintering time and temperature and affects sample poling, further investigation of the effects of sintering time and temperature is recommended to see if transducer performance can be enhanced. The effects of porosity with sintering time and temperature and transducer performance should also be investigated.

2. **Investigate adhesion of tranducers to substrates**

This can partly be included as research to follow the previous recommendation. Sintering times and temperatures will most likely affect adhesion of bismuth titanate to various substrates so this is another area that requires further investigation. Another effect worth investigating is the effect thermal cycling will have on adhesion. Measuring the linear coefficient of thermal expansion of bismuth titanate would also give a better indication of materials may be well suited for substrates.

3. Understand changes in dispersive behavior with temperature

Chapter 4 demonstrated that that a systems dispersion can be fairly sensitive to temperature. Further modeling and analysis of such systems will be necessary if practical analysis of structures in similar situations is to be realizable.

4. Test Rayleigh wave generation at elevated temperatures

The results for Lamb wave generation at elevated temperatures were presented in Chapter 4. Since generation of Lamb waves and Rayleigh waves are similar in nature it is believed that the operating temperature range for Rayleigh waves will not differ much from Lamb waves; however this hypothesis still warrants experimental verfication.

5. Measure bismuth titanate's emmsivity

Temperature measurements during sintering in this work were done with an optical pyrometer. More accurate temperature measurments of samples can be made with IR thermometers if the emmisivity of the material is known.

Bibliography

1. Hayt Jr., William, Buck, John A.(2001) *Engineering Electromagnetics*. New York, NY: McGraw-Hill.

2. Uchino, Kenji.(2000). *Ferroelectric Devices*.New York, NY: Mercel Dekker, Inc.

3. Searfass, Cliff. (2005). *Design and Fabrication of High Frequency Piezoelectric Pulse Transformers*. Undergraduate Thesis, The Pennsylvania State University.

4. Wei, Chong Cheong, Yahaya, Muhammad, and Salleh, Muhammad Mat. Bismuth Titanate. (2004). Thin Film for Pressure Sensor Prepared By Sol Gel Method. *IEEE International Conference on Semiconductor Electronics (7)*,(597-600).

5. Cady, Walter Guyton. (1964). *Pieozelectricity: An Introduction to the Theory and Applications of Electromechanical Phenomena in Crystals.* New York, NY: Dover Publicatoins, Inc.

6. Nye, J.F. *Physical Properties of Crystals*. Oxford: Clarendon Press.

7. Rosen, Carol Zwick. (1992). *Piezoelectricity.* Springer1992.

8. Yang, Jiashi.(2005).*An Introduction to the Theory of Piezoelectricity*. New York, NY: Springer.

9. Philips, James R. *Piezoelectric Technology Primer*. CTS Corp. Technology Components. 20 Nov. 2005. <http://www.ctscorp.com/components/piezoelectric.htm>.

10. Lord Rayleigh. (1885). On Waves Propagated Along the Plane Surfaces of an Eleastic Solid. *Proceedings of the London Mathematical Society, (17).*(4-11).

11. Viktorov, Igor Aleksandrovich. (1967). *Rayleigh and Lamb Waves: Physical Theory and Application.* New York, NY:Plenum Press.

12. Bergmann, L. *Ultraschall und seine Anwendung in Wissenschaft und Technik*. Ann Arbor, MI: Edwards.

13. Lamb, H. (1917). On Waves in an Elastic Plate. *Proc. Roy. Soc London. (93)* (114). 1917.

14. Aatre, Kiran R (2004). *Design of Inter-Digital Transducers and MEMS Based Lamb Wave Sensors for Health Monitoring of Structures*. Ph. D. Thesis. The Pennsylvania State University.

15. Rose, Joseph L. (1999) *Ultrasonc Waves in Solid Media.* Cambridge UK: Cambridge University Press.

16 Aurivilius, B.(1949). Mixed Bismuth Oxides with Layer Lattices II. Strucure of $Bi_4Ti_3O_{12}$. *Arkiv Kemi*, *(1)*.

17 Lazarevic, Z., Stojanovic, B.D., Varela, J.A. (2005) An Approach to Analyzing Synthesis, Structure, and Properties of Bismuth Titanate Ceramics. *Science of Sintering*. *(37)*. (199-216).

18. Smolenskii, G.A., Bokov, V.A., Isupov, V.A., Kranik, N.N., Pasynkov, R.E., Sokolov A.I.(1984). *Ferroelectrics and Related Materials.* New York, NY: Gordon and Breach Science Publishers.

19. Cummins, E. Cross, L.E.(1968). Crystal Symmetry, Optical properties and Ferroelectric Polarization of $Bi_4Ti_3O_{12}$ Single Crystals. *J. Appl. Phys. 39(5)*. 1968.

20. Dorrian, J.F., Wolfe, R.W., Newnham, R.E. (1971). Crystal Structure of $Bi_4Ti_3O_{12}$. *Ferroelectrics*,*(3)*.(17-27).

21. Shulman, H., Testorf, M., Damjanovic, D., Setter, N.(1996). Microstructure, Electrical Conductivity, and Piezoelectric Properties of Bismuth Titanate. *J. Am. Cer. Soc*. *79(12)*..

22. Vollegas, M., Caballero, A.C., Moure, C., Duran, P., Fernandez, J.F., (1999). Factors Affecting the Electrical Conductivity of Donor-doped $Bi_4Ti_3O_{12}$ Piezoelectric Ceramics. *J. Am. Cer. Soc. 82 (9)*..

23. Ng, S.H., Wang,J., Xue, J.M. (2002). Bismuth Titanate from Mechanical Activation of a Chemically Coprecipitated Precursor. *J. Am. Cer. Soc. 85 (11)*..

24. Ohring, M.(1992). *The Materials Science of Thin Films.* San Diego, CA: Academic Press.

25. Sedlar, M, Sayer, M. (1996) Structural and Electrical Properties of Ferroelectric Bismuth Titanate Thin Films Prepared by the Sol-gel Method. *Ceramic Intl*, *(22)*, (241-47).

26. Fuierer, P, Li, B. Nonepitaxial Orientation in Sol-gel Bismuth Titanate. *J. Am. Ceram. Soc. 85(2)*. (299-304).

27. Joshi, P.C., Krupanidhi, S.B. (1997). Structure and Electrical Studies on Rapid Thermally Processed Ferroelectric $Bi_4Ti_3O_{12}$ by Metallo-organic Solution Deposition. *J. Appl. Phys.(34*). (5193-97).

28. Sun, S. (1997) *Ferroelectric Thin Films: Part I, An Investigation of Self Polarization and Related Phenomena; Part II, Chemical Deposition of c-axis Oriented Bismuth Titanate.*Ph. D. Thesis. New Mexico Institute of Mining and Technology. Socorro, NM.

29. Kobayashi, M. Jen, C.-K., Ono, Y., Kruger, S. (2004). Lead Free Thick Piezoelectric Films as Miniature High Temperature Ultrasonic Transducers. *IEEE Ultrasonics Symposium.* (910-913).

30. Sutton, Willard H. Microwave Processing of Ceramic Material. In Clark, David E., Folze, Diane C., Folgar, Carlos E., Mahmoud, Morsi M. (Ed.), *Microwave Solutions for Ceramic Engineers*.. Westport, OH: The American Ceramic Society. (35-66)

31. Clark, D.E, Folz, D.C. What is Microwave Processing? In Clark, David E., Folze, Diane C., Folgar, Carlos E., Mahmoud, Morsi M. (Ed.), *Microwave Solutions for Ceramic Engineers*.. Westport, OH: The American Ceramic Society. (1-34)

32. Schiffmann, Robert F. Principles of Industrial Microwave Heating. In Clark, David E., Folze, Diane C., Folgar, Carlos E., Mahmoud, Morsi M. (Ed.), *Microwave Solutions for Ceramic Engineers*.. Westport, OH: The American Ceramic Society. (67-86)

33. Kozuka, Hiromitsu, Sakka, Sumio.(2005). *Handbook of sol-gel science and technology: processing, characterization, and applications – Volume 1: Sol-gel processing.* Norwell, MA: Kluwell Academic Publishers.

34. Reed, James. (1995). *Principles in ceramic processing, 2nd ed.* John Wiley & Sons, Inc.

35 Joshi, P.C., Mansingh, Abhay, Kamalasanan, M.N., Chandra, Subhas. (1991). Strucutural and optical properties of ferroelectric $Bi_4Ti_3O_{12}$ thin films by sol-gel technique. *Appl. Phys. Lett 59 (19),* 2389-90.

36 Sun, Shan. (April, 1997). *Ferroelectric thin films: part I, an investigation of sel-polarization and related phenomena in PZT; Part II, chemical deposition of c-axis oriented bismuth titanate.* Ph.D. Thesis. New Mexico Institute of Mining and Technology, Socorro, NM.

37. Kobayashi, M., Jen, C.-K., Ono, Y., Krüger, S.(2004). Lead free piezoelectric thick films as miniature high temperature ultrasonic transducers. *IEEE Ultrasonics Symposium*, *2 (23)*. (910-913).

38. Patnaik, Prayodt.(2003). *Handbook of Inorganic Chemicals*. New York, NY: McGrawn-Hill Handbooks.

39. Morozov, M.I., Mezentseva, L.P., Gusarov, V.V. (2002) Mechanism of formation of $Bi_4Ti_3O_{12}$. *Russian Journal of General Chemistry, 72 (7),* 1110-13.